Nanocluster Size-Control and "Magic Number" Investigations. Experimental Tests of the "Living-Metal Polymer" Concept and of Mechanism-Based Size-Control Predictions Leading to the Syntheses of Iridium(0) Nanoclusters Centering about Four Sequential Magic Numbers†

Murielle A. Watzky and Richard G. Finke*

Department of Chemistry, Colorado State University, Fort Collins, Colorado 80523

Received June 19, 1997. Revised Manuscript Received August 18, 1997[⊗]

Our recent kinetic and mechanistic studies of the formation of Bu_4N^+ and $P_2W_{15}Nb_3O_{62}^{9-}$ polyoxoanion-stabilized $Ir(0)_{\sim 300}$ nanoclusters led to the elucidation of a new mechanism for nanoclusters synthesized from metal salts under H_2: slow, continuous nucleation, rate constant k_1, then autocatalytic surface growth, rate constant k_2. This mechanism contains four key, previously unverified predictions: (i) that the nanoclusters are "living-metal polymers" and, hence, that a series of increasing size nanoclusters can be synthesized by design; (ii) that the ratio of rates of growth to nucleation, R (=k_2[nanocluster active sites]/k_1), should correlate with and should be useful *to predict* the size of new nanoclusters; (iii) that the autocatalytic surface growth should tend to favor so-called "magic-number" size (i.e., closed shell; higher stability) nanoclusters; and, overall, (iv) that it should be possible to prepare, for the first time, a sequential series of nanoclusters centering about the transition metal magic-number nanocluster sizes, M_{13}, M_{55} M_{147}, M_{309}, M_{561}, M_{923} (and so on). These mechanism-based predictions are tested via the present work. The end result is the synthesis of an unprecedented *sequential series* of $Ir(0)_n$ nanocluster distributions centering about four sequential transition-metal magic numbers, specifically $Ir(0)_{\sim 150}$, $Ir(0)_{\sim 300}$, $Ir(0)_{\sim 560}$, and $Ir(0)_{\sim 900}$. Also discussed is another, as-yet unverified, prediction of the autocatalytic surface-growth mechanism and its living-metal polymer phenomenon, namely, that one can in principle rationally design and then synthesize all possible geometric isomers of bi-, tri-, and higher multimetallic transition-metal nanoclusters, each in an initially known, layered, "onionskin" structure.

Introduction

The rational control of the size of a given nanocluster[1] is an important and often cited[2] but generally unattained goal[2b,3] in modern nanocluster science (see Reetz's electrochemical method, however[3g]). In recent mechanistic work on the formation of novel polyoxoanion- and Bu_4N^+-stabilized $Ir(0)_{\sim 300}$ nanoclusters[4,5] (Figure 1), we uncovered evidence for the two-pseudoelementary-step[4b] pathway in Scheme 1, consisting of (a) slow, continuous nucleation (steps 1−3) and then (b) autocatalytic surface growth (step 4). This new mechanism accounts *quantitatively* for the time dependence of the formation of the $Ir(0)_{\sim 300}$ nanoclusters.[4a,b]

The success of this simple kinetic scheme and minimum mechanism in accounting for a "self-assembly"[6] reaction that must involve *at least* 300 steps (see the observed stoichiometry, shown at the bottom of Scheme 1) is impressive. This simple, two-step kinetic scheme works because the autocatalytic surface-growth step is repeated many times and because the other steps present are "fast" (i.e., fast vs the kinetically crucial k_1 and k_2 steps). Our earlier kinetic and mechanistic work[4] is also a relatively rare kinetic and mechanistic study of a self-assembly reaction in materials chemistry.[6]

† Part III in a series on Nanocluster Formation Mechanistic Studies. For parts I−V in this series, see ref 4.

⊗ Abstract published in *Advance ACS Abstracts,* October 1, 1997.

(1) Lead reviews on nanoclusters: (a) *Physics and Chemistry of Small Clusters*; Jena, P., Rao, B. K., Khanna, S. N., Eds.; Plenum Press, New York, 1987. (b) Andres, R. P.; Averback, R. S.; Brown, W. L.; Brus, L. E.; Goddard, W. A.; Kaldor, A.; Louie, S. G.; Moscovits, M.; Peercy, P. S.; Riley, S. J.; Siegel, R. W.; Spaepen, F.; Wang, Y. *J. Mater. Res.* **1989**, *4*, 704 (a Panel Report from the United States Department of Energy, Council on Materials Science on "Research Opportunities on Clusters and Cluster-assembled Materials"). (c) Thomas, J. M. *Pure Appl. Chem.* **1988**, *60*, 1517. (d) Henglein, A. *Chem. Rev.* **1989**, *89*, 1861. (e) A superb series of papers, complete with a record of the insightful comments by the experts attending the conference, is available in: *Faraday Discuss.* **1991**, *92*, 1−300. (f) Bradley, J. S. In *Clusters and Colloids. From Theory to Applications*; Schmidt, G., Ed.; VCH Publishers: New York, 1994; pp 459−544. (g) Schmid, G. In *Aspects of Homogeneous Catalysis*; Ugo, R., Ed.; Kluwer: Dordrecht, 1990; Vol. 7, Chapter 1. (h) Henglein, A. *J. Chem. Phys.* **1993**, *97*, 5457. (i) Belloni, J. *Curr. Opin. Colloid Interface Sci.* **1996**, *1*, 184. (j) A list of more than 80 lead references is compiled in: Bönnemann, K.; Braun, G.; Brijoux, W.; Brinkmann, R.; Schulze Tilling, A., Seevogel, K.; Siepen, K. *J. Organo. Met. Chem.* **1996**, *520*, 143.

(2) (a) In 1989, a DOE panel report concluded (see p 705 in ref 2b) that "Present methods for the synthesis of useful amounts of size-selected (nano)clusters...are almost nonexistent." For other quotes from the literature demonstrating that size control is a major, often stated objective in current nanocluster science see the citations in footnotes 5 and 7 elsewhere.[4b] (b) Andres, R. P.; Averback, R. S.; Brown, W. L.; Brus, L. E.; Goddard, W. A., III; Kaldor, A.; Louie, S. G.; Moscovits, M.; Peercy, P. S.; Riley. S. J.; Siegel, R. W.; Spaepen, F.; Wang, Y. *J. Mater. Res.* **1989**, *4*, 704. (c) Professor Reetz's electrochemical synthesis of transition-metal nanoclusters is noteworthy: Reetz, M.; Helbig, W. *J. Am. Chem. Soc.* **1994**, *116*, 7401.

S0897-4756(97)00438-9 CCC: $14.00

A good mechanism not only (a) explains all the observed data, as the mechanism in Scheme 1 does

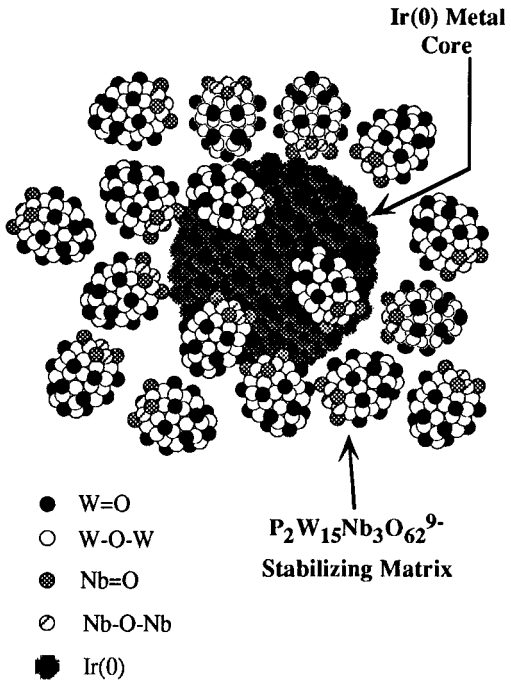

Figure 1. Idealized, roughly-to-scale representation of a $P_2W_{15}Nb_3O_{62}^{9-}$ polyoxoanion and Bu_4N^+ stabilized $Ir(0)_{\sim 300}$ nanocluster, $[Ir(0)_{\sim 300}(P_4W_{30}Nb_6O_{123}^{16-})_{\sim 33}](Bu_4N)_{\sim 300}Na_{\sim 228}$. The Ir(0) atoms are known (by electron diffraction) to be cubic-closed packed as shown.[5b] For the sake of clarity, only 17 polyoxoanions are shown, the polyoxoanion is shown in its monomeric, $P_2W_{15}Nb_3O_{62}^{9-}$ form (and not as its Nb−O−Nb bridged, anhydride form), and the ~300 Bu_4N^+ and ~228 Na^+ cations have been deliberately omitted.

(including a number of previously unexplained litera ture observations of induction periods and "burst"—that is, autocatalytic—formation of nanoclusters[4b]), but also (b) *makes predictions that can be experimentally tested and thus verified or refuted*. Four predictions of the mechanism in Scheme 1 are (i) that nanoclusters such as $Ir(0)_{\sim 300}$ are in fact "living-metal polymers"[7] from which larger size nanoclusters can be grown simply by adding more metal precursor (while also controlling the relative rates of the autocatalytic growth vs the nucleation of new nanoclusters, so that little to no new nucleation occurs); and (ii) that the $k_2[B]/k_1$ ratio should correlate with, and thus can be used to predict and to control, nanocluster size (i.e., a smaller k_1 and/or a larger $k_2[B]$ give rise to a larger $k_2[B]/k_1$ ratio, which in turn should correlate with the formation of larger nanoclusters, while a smaller $k_2[B]/k_1$ ratio should correlate with the formation of smaller nanoclusters). In addition, the mechanism in Scheme 1 predicts (iii) that closed shell, "magic-number" nanoclusters might be favored since their intrinsic greater thermodymanic stability can, at least in principle, lead to a lower kinetic reactivity for surface growth; and thus (iv) that it should be possible, *by design*, to synthesize distributions of nanoclusters centering at least approximately about the magic numbers for transition-metal nanoclusters, that is, M_{13}, M_{55} M_{147}, M_{309}, M_{561}, M_{923} and so on.

The synthesis of a sequential series of magic-number nanoclusters carried out as part of the present study is illustrated in Figure 2. In this work, the synthesis of a

(3) (a) An apparent exception to this general statement is the reverse-micellar-template syntheses of especially semiconductor nanoclusters, syntheses which produce near-monodisperse nanoclusters at a record ±5−10% size dispersion (i.e., ca. 2−3-fold better than typically seen in an *unoptimized* autocatalytic surface-growth pathway). However, and although it is possible to control micellar *size* and even shape by the use of different size, preformed reverse micelles,[3b] this has not yet been *experimentally* demonstrated in a more general fashion for nanoclusters, and especially not for transition-metal nanoclusters[3e] (probably, at least in part due to the poor understanding of the nanocluster mechanism of formation in such micellar systems[3d]). In addition, more recent work by Pileni and co-workers indicates that *it is not possible to control simultaneously:* (i) size, (ii) polydispersity *and* (iii) composition of at least Cu/Cu_xO_y nanocolloids using reverse micelles.[3e] This statement follows since size control is sensitive to the amount of water, but at higher water content the polydispersity and amount of Cu_xO_y clusters increases (i.e., in comparison to the Cu(0) clusters). (b) See Tables 1 and 2 in: Maitra, A. *J. Phys. Chem.* **1984**, *88*, 5122. Naza'rio, L. M. M.; Hatton, T. A.; Crespo, P. S. G. *Langmuir*, **1996**, *12*, 6326. A review of the surfactant AOT (sodium bis(2-ethylhexyl)sulfosuccinate) and its reverse micelles: De, T. K.; Maitra, A. *Adv. Colloid Interface. Sci.* **1995**, *59*, 95. (c) The following authors note that "the shape of these aggregates (reverse micelles) depends on several factors and generally changes from spherical to cylindrical to more complex structures according to the nature of the surfactant counterion (for ionic surfactants), the surfactant, and the water concentration." Sangregorio, C.; Galeotti, M.; Bardi, U.; Baglioni, P. *Langmuir* **1996**, *12*, 5800 and references therein. (d) Steigerwald and Brus discuss some of the achievements and the limitations—including the lack of mechanistic understanding—in the use of structured reaction media to provide quite useful, but not yet "on demand", size control in semiconductor nanocluster syntheses: Steigerwald, M. L.; Brus, L. E. *Acc. Chem. Res.* **1990**, *22*, 183. (e) Lisiecki, I.; Pileni, M. P. *J. Am. Chem. Soc.* **1993**, *115*, 3887. Lisiecki, I.; Pileni, M. P. *J. Phys. Chem.* **1995**, *99*, 5077. Lisiecki, I.; Billoudet, F.; Pileni, M. P. *J. Phys. Chem.* **1996**, *100*, 4160. (f) Of note is Wilcoxon's *nonaqueous* inverted micellar syntheses of near-monodisperse Au, Ag, MoS_2, Fe nanoclusters (and brief claim of Co, Ni, Pd, Pt, and Ir nanoclusters). The range of specific systems includes (i) $CH_3(CH_2)_n(CH_2CH_2O)_mOH$ surfactant/hexane, octane and other "oils" (as solvent); (ii) anionic AOT {Na^+-[bis(2-ethylhexyl)sulfosuccinate)-}/toluene as the "oil"; and (iii) $(C_{12}H_{25})_2NMe_2^+X^-$ (X = Br, Cl)/hexane/hexanol: Wilcoxon, J. P.; Williamson, R. L.; Braughman, R. *J. Chem. Phys.* **1993**, *98*, 9933. Wilcoxon, J. P.; Martino, A.; Braughman, R.; Klavetter, E.; Sylwester, A. P. *Mater. Res. Soc. Symp.* **1994**, *351*, 311. Venturini, E. L.; Wilcoxon, J. P.; Newcomer, P. P. *Mater. Res. Soc. Symp.* **1993**, *286*, 131. Wilcoxon, J. P.; Samara, G. A. *Phys. Rev. B* **1995**, *51*, 7299. This work provides detailed insights into experimental variables one must control in these systems to obtain the best, reproducible nanoparticles (e.g., the removal of water, oxygen, and sources of inhomogeneous nucleation such as gas bubbles or dust particles). (g) Electrochemical growth of nanoclusters where size can be controlled by the overpotential and currrent density is described elsewhere[2c] by Reetz.

(4) (a) Part I: Watzky, M. A.; Aiken, J. D. III; Widegren, J.; Finke, R. G., submitted ("A New Kinetic Method to Follow Transition-Metal Nanocluster Formation Based on Catalytic Activity and the Pseudo-elementary Step Concept"). (b) Part II: Watzky, M. A.; Finke, R. G. *J. Am. Chem. Soc.*, in press ("Transition Metal Nanocluster Formation Kinetic and Mechanistic Studies. A New Mechanism When Hydrogen Is the Reductant: Slow, Continuous Nucleation and Fast Autocatalytic Surface Growth"). (c) Part IV: Aiken, J. D. III; Finke, R. G.; *J. Am. Chem. Soc.*, in press ("Nanocluster Formation Synthetic, Kinetic and Mechanistic Studies. The Discovery of, and Then Methods To Avoid, Hydrogen Mass-Transfer Limitations in the Synthesis of Polyoxoanion- and Tetrabutylammonium- Stabilized 40 ± 6 Å $Rh(0)_{\sim 2400}$ Nanoclusters"). (d) Part V: Widegren, J.; Watzky, M. A.; Finke, R. G., experiments in progress. (e) For a review of polyoxoanion and Bu_4N^+ stabilized $Ir(0)_{\sim 300}$ and $Ir(0)_{\sim 900}$ nanoclusters, plus definitions of terms such as "colloids and nanocolloids vs nanoclusters", "near-monodisperse", and other useful terms, see: Aiken, J. D. III; Lin, Y.; Finke, R. G. *J. Mol. Catal. A: Chem.* **1996**, *114*, 29.

(5) (a) Lin, Y.; Finke, R. G. *Inorg. Chem.* **1994**, *33*, 4891. (b) Lin, Y.; Finke, R. G. *J. Am. Chem. Soc.* **1994**, *116*, 8335.

(6) One definition of self-assembly is simply "those processes in which humans are not actively involved" and, therefore, would include the *covalently* bonded Ir(0) nanoclusters prepared herein. Another definition is "the spontaneous association of molecules under equilibrium conditions into stable, structurally well-defined aggregates joined by *noncovalent bonds*",[6b] a definition that would exclude nanoclusters. (a) Whitesides, G. M. *Sci. Am.* **1995**, *Sept*, 146. (b) Whitesides, G. M.; Mathias, J. P.; Seto, C. T. *Science* **1991**, *254*, 1312 and references therein. (c) A review of organic and bioorganic self-assembly, one that reveals the dearth of kinetic and mechanistic studies: Philip, D.; Stoddart, J. F. *Angew. Chem., Int. Eng. Ed.* **1996**, *35*, 1154 and references therein. (d) Dagani, R. in *Chem. Eng. News*, **1996**, *July 8*, 26.

(7) Classic organic anionic living polymerization: (a) Szwarc, M. *Nature* **1956**, *178*, 1168. (b) Szwarc, M. In *Advances in Polymer Science*; Springer-Verlag: Berlin, 1983; Vol. 49.

Scheme 1. Minimum Mechanism[4b,5] for the Formation of Ir(0) Nanoclusters Consisting of (a) Slow, Continuous Nucleation (Steps 1−3), Rate Constant k_1 for the Pseudoelementary Step A → B, followed by (b) Fast Autocatalytic Surface Growth (Step 4), Rate Constant k_2 for the Pseudoelementary Step A + B → 2B.[a] Nucleation and Growth Are *Separated in Time* Since $k_1 \ll k_2$[B], Which in Turn Is a Key to the Observed Formation of a Near-Monodisperse[4e] (±≤15%) Particle Size Distribution

(a) Nucleation

$$A \xrightarrow{k_1} B$$

(1) $(COD)Ir(P_2W_{15}Nb_3O_{62})^{8-} + 2$ acetone $\rightleftharpoons (COD)Ir(acetone)_2^{+} + P_2W_{15}Nb_3O_{62}^{9-}$

(2) $(COD)Ir(acetone)_2^{+} + 2.5\ H_2 \rightarrow Ir(0) + H^+ +$ (S) $+ 2$ acetone

(3) $n\ Ir(0) \rightarrow Ir(0)_n$

(b) Autocatalytic Surface Growth

$$A + B \xrightarrow{k_2} 2B$$

(4) $(COD)Ir(P_2W_{15}Nb_3O_{62})^{8-} + 2.5\ H_2 + Ir(0)_n \rightarrow Ir(0)_{n+1} + H^+ + P_2W_{15}Nb_3O_{62}^{9-} +$ (S)

Net reaction:

$$300\ [(COD)Ir^{I}(P_2W_{15}Nb_3O_{62})^{8-}] + 750\ H_2 \longrightarrow Ir(0)_{300} + 300\ P_2W_{15}O_{62}^{9-} + 150\ H^+ + 300\ (S)$$

[a] Note that in step (4), the autocatalysis has a stoichiometry of $n \rightarrow n + 1$ [i.e., n (surface atoms) → $n + 1$ (surface atoms)] and not $1 \rightarrow 2$ as in the most basic form of autocatalysis (A + B → 2B) shown in Scheme 1. As detailed elsewhere,[4b] this introduces a "scaling" correction factor to the $k_{2,obsd}$ values, but otherwise has no effect on the autocatalytic kinetics.

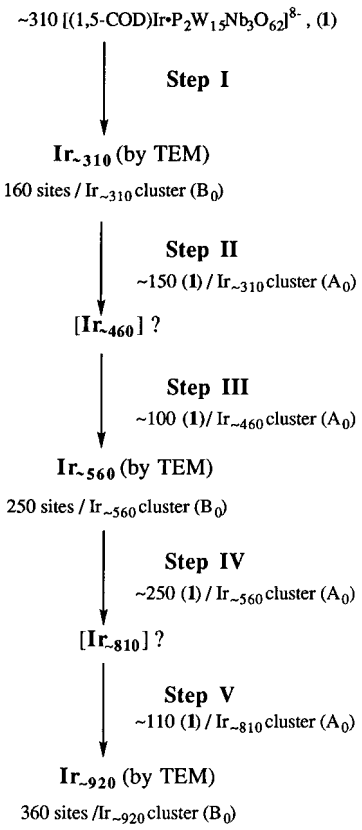

Figure 2. Living metal-polymer based synthetic scheme for the preparation of a series of $Ir(0)_n$ nanoclusters centering about sequential magic numbers, using a sequence of autocatalytic surface-growth steps and beginning with the known $Ir(0)_{\sim 300}$ seed. (The definitions of A_0 and B_0, and their significance, will become apparent later in the paper.) Transmission electron microscopy (TEM) analyses are performed at every other step in Figure 2 to stay above the TEM size-change detection limit of ca. ±5 Å.

series of $Ir(0)_n$ nanoclusters beginning from our *known*[4b,5] $Ir(0)_{\sim 300}$ "seeds" is experimentally investigated.

Note that perhaps the main limitation of such a scheme is the general lack of availability of the smallest possible seed, in the present example the currently unknown, presumably less stable $Ir(0)_{\sim 13}$ or $Ir(0)_{\sim 55}$.[8] Another important factor is that one needs to use a nanocluster seed that is as close to monodisperse as possible, for example, the typically near-monodisperse (≤±15%)[4e] size distribution that is available from our $Ir(0)_{\sim 300}$ preparation.[5]

Herein we report experimental tests of the mechanism-based predictions cited above; specifically, we report the results: (i) that $Ir(0)_n$ nanoclusters are indeed "living-metal polymers" from which larger size nanoclusters can be grown; (ii) that the k_2[B]/k_1 ratio does correlate semiquantitatively with, and thus can be used to predict and control, nanocluster size; (iii) that magic-number size nanoclusters are, in fact, a natural consequence of—and thus offer further experimental support for—surface autocatalytic growth; and (iv) that it is possible to design and synthesize, for the first time, distributions of nanoclusters centering about a series of the magic numbers, specifically $Ir(0)_{\sim 150}$, $Ir(0)_{\sim 300}$, $Ir(0)_{\sim 560}$, and $Ir(0)_{\sim 900}$. Hence the work reported herein also (v) provides the first use of a mechanism-based insight to control nanocluster size,[9] and (vi) provides additional evidence in support of the mechanism in

(8) The $Ir(0)_{\sim 13}$ and $Ir(0)_{\sim 55}$ are almost surely less stable than the higher magic numbers due to their greater proportion of surface Ir(0) atoms and thus fewer stabilizing, ca. 26 kcal/mol[28] Ir(0)-Ir(0) metal−metal bonds per Ir(0) present in these smaller nanoclusters.

(9) (a) Schmid, G.; West, H.; Malm, J.-O.; Bovin, J.-O.; Grenthe, C. *Chem. Eur. J.*, **1996**, *2*, 147 and references therein. Note that these authors use the "seed growth" method to prepare bimetallic nanoclusters. (b) Michel, J. B.; Schwartz, J. T. In *Catalyst Preparation Science*; Delmon, B., Grange, P., Jacobs, P. A., Poncelet, G., Eds.; Elsevier: New York, 1987; Vol. IV, pp 669−687. (c) Steigerwald, M. L.; Brus, L. *Acc. Chem. Res.* **1990**, *23*, 183. These authors specifically note the concept of "living polymers" (see p 184) in the case of their CdSe or CdS nanoclusters. (d) Klabunde also has noted the analogous "living colloidal palladium" concept: Cardenas-Trivino, G.; Klabunde, K. J.; Dale, E. B. *Langmuir* **1987**, *3*, 986. Franklin, M. T.; Klabunde, K. J. In *High Energy Processes in Organometallic Chemistry*; Suslick, K. S., Ed.; ACS Symposia Series 333; American Chemical Society, Washington, DC, 1987; Chapter 15, p 246. (e) Transition-metal magic numbers nanoclusters: see refs 26 and 27 provided as part of the present paper. (f) Klots, T. D.; Winter, B. J.; Parks, E. K.; Riley, S. J. *J. Chem. Phys.* **1990**, *92*, 2110. (g) Although not noted as a "living metal polymer system", this concept—and probably also the surface autocatalytic growth mechanism that we have uncovered[4]—probably underlies the preparation of a narrower size distributions of Ni heterogeneous catalysts: Che, M.; Cheng, Z. X.; Louis, C. *J. Am. Chem. Soc.* **1995**, *117*, 2008.

Scheme 1 and, therefore, its other predictions and ramifications. One such prediction, discussed toward the end of this paper, is how to control size, composition, and initial structure in bi- and higher multimetallic nanoclusters.

It is important to note, for the proper integration of this work into the existing literature, that the concept of "seed-" or "germ"-initiated growth of nanoclusters is not new and, as Schmidt has recently pointed out,[9a] has been used in heterogeneous catalysis since 1906.[9b] Also, the term "living polymer"[7] has been used previously in the context of nanoclusters by Steigerwald and Brus[9c] and by Klabunde.[9d] However, there has been no previous mechanistic understanding behind such studies (i.e., such as Scheme 1) nor any mechanistic understanding of, for example, how or why magic-number sized nanoclusters tend to form. Moreover, nothing has previously appeared analogous to the mechanism-based prediction, and then experimental preparation, of a series of nanoclusters centering about four consecutive magic numbers.[10]

Experimental Section

(A) Materials. Acetone was purchased from Burdick & Jackson (water content <0.2%) and stored in a Vacuum Atmospheres drybox. Cyclohexene (Aldrich, 99%) was purified by distillation from Na under Ar and stored in the drybox. The nanocluster precursor complex $[Bu_4N]_5Na_3[(1,5\text{-COD})Ir(P_2W_{15}Nb_3O_{62})]$ (**1**)[11] and the polyoxoanion $[Bu_4N]_9[P_2W_{15}Nb_3O_{62}]$ (**2**)[12] were prepared according to our literature procedures, and stored in the drybox.

(B) Hydrogenations. *(1) Apparatus.* The nanocluster formation and hydrogenation reactions were carried out as previously described in detail,[5a] in a Fischer−Porter bottle modified with Swagelock TFE-sealed Quick-Connects and connected to a H_2 line and an Omega PX-621 pressure transducer interfaced through an Omega WB-35 A/D converter to an IBM PC-XT, using the RS-232 module of Lotus Measure (see Figure 6 elsewhere for a drawing and further details of this hydrogenation apparatus).[5a] The progress of an individual hydrogenation reaction was monitored by the loss of H_2 pressure (over periods ranging from 1 to 60 h), and the data were then fed into, and worked up via, Lotus 1-2-3. Five types of control experiments were done previously to ensure that the apparatus provided both a precise and accurate picture of the H_2 uptake reaction[5a] (i.e., controls showing that it did not admit detectable atmospheric O_2 (≪1 mM) and that it reproduced faithfully the literature rate for a known hydrogenation catalyst; that the apparatus did not leak appreciable H_2 pressure; plus other controls as well[5a]).

*(2) Standard Conditions. Nanocluster Formation and Cyclohexene Hydrogenation with **1** as Precatalyst.* A typical standard conditions experiment followed closely our established protocol.[5a] In the drybox, 20.5 ± 1.0 mg (3.61 ± 0.18 μmol) of the precatalyst complex $[Bu_4N]_5Na_3[(1,5\text{-COD})Ir(P_2W_{15}Nb_3O_{62})]$ (**1**) was dissolved in 2.5 mL of acetone, followed by the addition of 0.50 ± 0.03 mL (4.94 ± 0.30 mmol) of cyclohexene. The clear, bright-yellow solution (containing 1.20 ± 0.06 mM of **1** and 1.65 ± 0.10 M of cyclohexene) was then transferred to a clean, 22 × 175 mm disposable Pyrex culture tube containing a $^5/_8$ in. × $^5/_{16}$ in. magnetic stir bar. The tube was placed in a Fischer−Porter bottle modified with Swagelock TFE-sealed Quick-Connects (as described above); the bottle was then sealed and brought out of the drybox, and placed into a Fischer Scientific 9100 temperature-controlled (±0.1 °C) bath at 22.0 ± 0.1 °C unless otherwise indicated. In the meantime, the H_2 line and pressure transducer had been evacuated for at least 1 h under vacuum (≤100 mmHg) and then refilled with prepurified H_2, with the goal of removing trace oxygen and water from the apparatus and its lines. Next, the Fischer−Porter bottle was connected between the (now O_2 and H_2O free) pressure transducer and the H_2 line using the Quick-Connects. The Fischer−Porter bottle was then purged 15 times with approximately 40 psig H_2 (15 s/purge), the H_2 pressure was set to a desired value (typically 40 ± 0.5 psig) in less than 10 s, and the connection between the Fischer−Porter bottle and the H_2 line was closed (see Figure 6 provided elsewhere as needed).[5a] The Fischer−Porter bottle was shaken vigorously for 15 s (to equilibrate the gas and solution phases, thereby also initiating fully the hydrogenation reaction) and then was vortex stirred at 570 ± 30 rpm. The H_2 pressure vs time data collection was then started, with this time designated as $t = 0$.

*(3) Nanocluster Formation from the Nanocluster Precursor, **1**: Living-Metal Polymer Experiments.* The following series of experiments was performed using isolated $Ir(0)_n$•-{polyoxoanion} nanoclusters, which can act as "seeds" for further nanocluster growth. All solution transfers described below as "quantitative" were, however, done without the aid of added solvent, since the exact volume of solution is crucial (i.e., in yielding the resultant, exactly known millimoles of nanoclusters or nanocluster precursor, **1**).

Step I: The synthesis of the parent or "seed" $Ir(0)_{\sim 300}$ nanoclusters was accomplished exactly as described in the standard conditions section (hydrogenation time ≥ 17 h). Three separate experiments were performed and the resulting solutions were used in step II.

Step II. At the end of each of three separate runs of step I, the Fischer−Porter bottle was detached from the hydrogenation line via its Quick-Connects and brought back to the drybox, and its acetone solution was quantitatively transferred with a pipet into a 5 mL screw-capped vial, and the vial was then sealed for a short period of storage. Once all three step I runs had been performed, the three separate acetone solutions were transferred quantitatively via a pipet into a single 15 mL centrifuge tube. The centrifuge tube was then clamped to a ring-stand, and the dark-brown suspension of Bu_4N^+ and polyoxoanion-stabilized nanoclusters was allowed to separate over 1 h. (As discussed elsewhere,[5a] the nanoclusters are still soluble in, for example, fresh acetone, but precipitate during their synthesis and its concomitant cyclohexene hydrogenation due to the solution polarity decrease as 4.9 mmol of cyclohexene is reduced to 4.9 mmol of the less polar cyclohexane.) The light-brown supernatant was then carefully removed with a pipet. Immediately thereafter 3.0 mL of acetone were added to the dark-brown residue, and the residue was redissolved with gentle shaking. A preselected portion (1.0 mL) of this dark-brown acetone solution was transferred quantitatively via pipet into a clean, 3 mL centrifuge tube, and this sample was then used for TEM (see section E, TEM sample preparation). Next, 20.5 mg (3.61 μmol) of the precatalyst complex **1** were dissolved in 1.0 mL of acetone, followed by the addition of the remaining 2.0 mL of the dark-brown acetone solution.

(10) The closest examples we are aware of are the pioneering Russian work on "giant Pd clusters"[10a−c] and Chaudret, Bradley and co−workers Pd nanoclusters.[10d] From the Russian work, recipes are available leading to the following series of Pd nanoclusters, $Pd_{\sim 560}$, $Pd_{\sim 1400}$, and $Pd_{\sim 2000}$ corresponding to clusters centering about the 5, 7 and 8 shell magic numbers.[10a,b] A 4-shell, *platinum* ($Pt_{\sim 300}$) nanocluster is also known.[10c] Although the mechanism of formation of these clusters is unreported, we suspect that the underlying mechanism and principles therein are close to—if not exactly the same as—those we uncovered previously[4b] and now apply in the present paper. (a) $Pd_{\sim 560}$: Vargaftik, M. N.; Zagorodnikov, V. P.; Stolyarov, I. P.; Moiseev, I. I.; Kochubey, D. I.; Likholobov, V. A.; Chuilin, A. L.; Zamaraev, K. I. *J. Mol. Catal.* **1989**, *53*, 315 and references therein. Vargaftik, M. N.; Moiseev, I. I.; Kochubey, D. I.; Zamaraev, K. I. *Faraday Discuss.* **1991**, *92*, 13−29. (b) Schmid, G.; Emde, S.; Maihack, V.; Meyer-Zaika, W.; Peschel, St. *J. Mol. Catal. A: Chem.* **1996**, *107*, 95. (c) Pt∼309: Schmid, G.; Morun, B.; Malm, J.-O. *Angew. Chem., Int. Ed. Engl.* **1989**, *28*, 778. (d) The report of reproducible preparations of Pd carbonyl nanocluster distributions centering about the 2, 3, and 5 shell magic number clusters, $M_{\sim 55}$, $M_{\sim 147}$, and $M_{\sim 561}$: Amiens, C.; de Caro, D.; Chaudret, B.; Bradley, J.; Mazel, R.; Roucau, C. *J. Am. Chem. Soc.* **1993**, *115*, 11638. See also: Rodriguez, A.; Amiens, C.; Chaudret, B.; Casanove, M.-J.; Lecante, P.; Bradley, J. *Chem. Mater.* **1996**, *8*, 1978.

(11) Pohl, M.; Lyon, D. K.; Mizumo, N.; Nomiya, K.; Finke, R. G. *Inorg. Chem.* **1995**, *34*, 1413.

(12) Weiner, H. W.; Aiken, J. D. III; Finke, R. G. *Inorg. Chem.* **1996**, *35*, 7905.

This opaque brown solution was placed in a 22 × 175 mm disposable Pyrex culture tube containing a $^5/_8$ in. × $^5/_{16}$ in. magnetic stir bar. The culture tube was then placed in the usual Quick-Connect-equipped Fischer−Porter bottle, brought out of the drybox, and the reaction was started via the usual sequence of H_2 purges and then shaking (see the standard conditions cited above). The hydrogenation time was >21 h. The resulting solution was used in step III.

Step III. At the end of the above run in step II, the Fischer−Porter bottle was detached from the hydrogenation line and brought back to the drybox, and its acetone solution was transferred quantitatively into a clean, 3 mL centrifuge tube which was then clamped to a ring-stand. Since no suspension was present, a small amount (less than 20 drops) of anhydrous, degassed diethyl ether was added slowly (i.e., dropwise over 1 min, without stirring), at which point the solution became opaque. The dark-brown suspension was allowed to separate over 1 h. The light-brown supernatant was then carefully removed with a pipet. Immediately thereafter 3.0 mL of acetone were added to the dark-brown residue, and the residue was redissolved with gentle shaking. Next, 14.2 mg (2.50 μmol) of the precatalyst complex **1** were dissolved in the dark-brown acetone solution. The opaque brown solution was then placed in a 22 × 175 mm disposable Pyrex culture tube containing a $^5/_8$ in. × $^5/_{16}$ in. magnetic stir bar. The culture tube was then placed in the usual Quick-Connect-equipped Fischer−Porter bottle and brought out of the drybox, and the reaction was started via the usual sequence of H_2 purges and then shaking (see the standard conditions cited above). The hydrogenation time was >24 h. The resulting solution was used in step IV.

Step IV. At the end of the above run in step III, the Fischer−Porter bottle was detached from the hydrogenation line, brought back to the drybox, and its acetone solution was quantitatively transferred into a clean, 3 mL centrifuge tube which was then clamped to a ring-stand. Since no suspension was present, a small amount (less than 20 drops) of anhydrous, degassed diethyl ether was added slowly (i.e., dropwise over 1 min, without stirring), at which point the solution became opaque. The dark-brown suspension was allowed to separate over 1 h. The light-brown supernatant was then carefully removed by pipet. Immediately thereafter 3.0 mL of acetone was added to the dark-brown residue, and the residue was redissolved with gentle shaking. A portion (1.0 mL) of this dark-brown acetone solution was transferred quantitatively by pipet into a clean, 3 mL centrifuge tube and then used as a sample for TEM analysis (see section E, TEM sample preparation). Next, 20.5 mg (3.61 μmol) of the nanocluster precursor complex **1** was dissolved in 1.0 mL of acetone, followed by the addition of the remaining 2 mL of the dark-brown acetone solution. This opaque brown solution was placed in a 22 × 175 mm disposable Pyrex culture tube containing a $^5/_8$ in. × 5/16 in. magnetic stir bar. The culture tube was then placed in the usual Quick-Connect-equipped Fischer−Porter bottle and brought out of the drybox, and the reaction was started via the usual sequence of H_2 purges and then shaking (see the standard conditions cited above). The hydrogenation time was >23 h. The resulting solution was used in step V.

Step V. At the end of the above run in step IV, the Fischer−Porter bottle was detached from the hydrogenation line and brought back to the drybox, and its acetone solution was quantitatively transferred into a clean, 3 mL centrifuge tube which was then clamped to a ring-stand. Since no suspension was present, a small amount (less than 20 drops) of anhydrous, degassed diethyl ether was added slowly (i.e., dropwise over 1 min, without stirring), at which point the solution had become opaque. The dark-brown suspension was allowed to separate over 1 h. The light-brown supernatant was then carefully removed by pipet. Immediately thereafter 3.0 mL of acetone were added to the dark-brown residue, and the residue was redissolved with gentle shaking. Next, 11.6 mg (2.05 μmol) of the nanocluster precursor complex **1** were dissolved in the dark-brown acetone solution. The opaque brown solution was then placed in a 22 × 175 mm disposable Pyrex culture tube containing a $^5/_8$ in. × $^5/_{16}$ in. magnetic stir bar. The culture tube was then placed in the usual Quick-Connect-equipped Fischer−Porter bottle and brought out of the drybox, and the reaction was started via the usual sequence of H_2 purges and then shaking (see the standard conditions cited above). The hydrogenation time was > 22 h.

(4) Synthesis of Ir(0)$_{\sim 150}$ via the Effect of Excess Polyoxoanion. First, and while in search of a synthesis that would yield the smaller, Ir(0)$_{\sim 150}$ magic-number nanocluster, we surveyed the other nanocluster formation reactions that we had done[4] and used the R' ratio (see the Results and Discussion) to predict that the following conditions would yield the desired Ir(0)$_{\sim 150}$ nanocluster. Then the following synthesis was run.

In the drybox, 20.5 mg (3.61 μmol) of **1** was dissolved in 2.5 mL of acetone to give the usual clear, bright-yellow solution. An amount of $(Bu_4N^+)_9[P_2W_{15}Nb_3O_{62}]$, **2**, was added (173.0 mg, or 7.5 equiv vs **1**), followed by the addition of 0.50 mL (1.65 M) of cyclohexene. The solution was then transferred in the usual way to a separate culture tube, which was in turn placed in a Quick-Connects-equipped Fischer−Porter bottle. This reaction vessel was then brought out of the drybox, and the nanocluster formation and olefin hydrogenation reaction was started exactly as in the standard conditions section.

*(5) Nanocluster Formation and Cyclohexene Hydrogenation with **1** as Precatalyst: Effect of Low Temperature.* A solution of **1** in acetone was prepared exactly as detailed in the standard conditions section. The solution was brought out of the box and thermostated at 3.0 ± 0.1 °C, and the nanocluster formation and olefin hydrogenation reaction was started exactly as in the standard conditions section.

(C) Curve Fits of the Hydrogen Uptake Data (or, Equivalently, the Cyclohexene Loss Data). *(1) Curve-Fitting Program.* Curve-fitting of the hydrogen uptake data (or, equivalently, the cyclohexene loss, vide infra) was performed using a nonlinear regression subroutine (RLIN), available in the IMSL Statistical Library, which uses a modified Levenberg-Marquard algorithm.[13] Calculations were done on an IBM/AIX workstation. A FORTRAN program was written that (i) reads the list of input data points, (ii) defines the analytical expression to which the data points will be curve-fit (see eq 3), (iii) asks for initial guesses of the variables (k_1 and k_2), and then (iv) calls the appropriate RLIN subroutine. Calculated values of the variables are obtained as output, along with details on the regression. A range of initial guesses of the variables (i.e., the widest possible range of empirical initial guesses which still allowed the subroutine to converge) was employed in order to avoid local minima. As described elsewhere, a control was done using a calculated, "mock" data set to ensure that the program faithfully delivered back the k_1 and k_2 values used to generate the mock data set (the curve-fit k_1 and k_2 values were within ±0.1% of the true values).[4b]

(2) Data Handling. Since the pressure transducer follows the H_2 pressure above the solution, but since the hydrogen uptake via the cyclohexene hydrogenation reaction is of course in solution, these two were related by treating the hydrogen atmosphere above the solution as an "hydrogen reservoir".[14a] Also, when desirable, the H_2 loss was equivalently expressed in terms of the loss of cyclohexene loss via the established[4b,5a] 1:1 H_2 to cyclohexene stoichiometry[14c] (eq 1d). As done

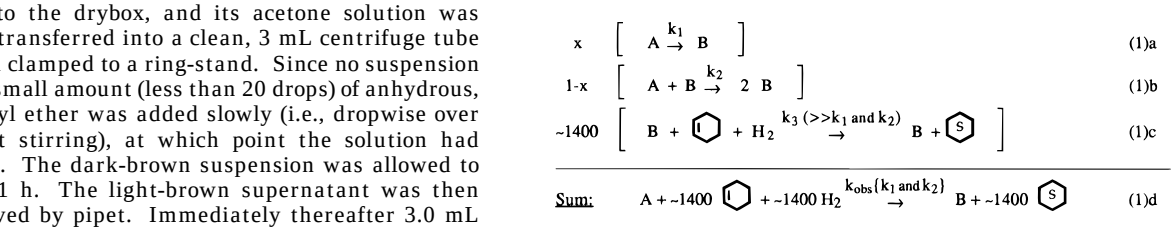

previously,[4b] only the data points prior to the consumption of half of the initial cyclohexene concentration were used in the curve-fitting process in order to ensure the validity of the pseudoelementary model.[15] The consumption of cyclohexene as a function of time was curve-fit to eq 3, yielding values of

k_1 and k_2.

$$-\mathrm{d[A]}/\mathrm{d}t = +\mathrm{d[B]}/\mathrm{d}t = k_1[\mathrm{A}] + k_2[\mathrm{A}][\mathrm{B}] \quad (2)$$

$$[\mathrm{A}]_t = \frac{(k_1/k_2) + [\mathrm{A}]_0}{1 + (k_1/k_2[\mathrm{A}]_0)\exp(k_1 + k_2[\mathrm{A}]0)t} \quad (3)$$

(3) Pseudoelementary Kinetic Model. The data points were curve-fit according to the previously derived pseudoelementary kinetic model below.[4a,b] Briefly, a "pseudoelementary step" is the sum of one or more kinetically slow elementary steps followed by any number of fast, non-rate-influencing elementary steps. The sum of these steps—by definition the pseudoelementary step—exhibits the stoichiometry of the sum reaction, but the kinetics of only the slow step(s), and thus is invaluable for the kinetic and mechanistic study of more complicated reactions such as the present, nanocluster formation reaction. For the original treatment of the kinetics which follow, plus lead references to the pioneering work of Noyes who developed this concept, see the text and ref 29 elsewhere.[4b]

In the above equations, A is the precatalyst (the nanocluster precursor, **1**), and B is the catalyst. The applicable rate equation is shown in eq 2.[4a,b]

The analytical expression that follows from integrating eq 2 is shown in eq 3.[4a,b]

(D) Transmission Electron Microscopy (TEM). *(1) Sample Preparation.* The solutions used for these TEM experiments were just those prepared and first run exactly as described above in the hydrogenations section. At the end of a given run (i.e., when 1 equiv of cyclooctane vs **1** had evolved as determined by the previously described GLC method[5b]), the Fischer−Porter bottle was detached from the hydrogenation line via its Quick-Connects and brought back into the drybox, and its acetone solution was quantitatively transferred by pipet into a clean, 5 mL centrifuge tube. The tube was then clamped to a ring-stand and the usual dark-brown suspension of Bu_4N^+- and polyoxoanion-stabilized nanoclusters was allowed to separate over 1−2 h. In some instances, the runs with an excess of added polyoxoanion or with no cyclohexene present as in the seed-growth experiments, no suspension was present. In those cases only, a small amount (usually <0.5 mL) of anhydrous, degassed diethyl ether was then added slowly (i.e., dropwise over 5 min), without stirring, until the solution became opaque but while halting the addition of ether before a precipitate is observed. After ca. 2 h of settling, the light brown supernatant was carefully removed by pipet, and the precipitate was allowed to dry overnight in the drybox.

The dry nanocluster samples in screw-capped vials were sent as *solids* to the University of Oregon for TEM. There, the addition of <0.25 mL of acetonitrile was performed, in air, just before the TEM analysis. Note that this transference of solids, rather than the original solutions, has been previously shown to be the preferable TEM-sample-transport method.[4b]

(2) Sample TEM Analyses. TEM analyses were performed as before[4,5] at the University of Oregon, via the expert assistance of Dr. Eric Schabtach, using the sample preparation procedure, and using a Philips CM-12 TEM with a 70-μm lens operating at 100 kV and with a 2.0 Å point-to-point resolution, all as previously described in detail.[5b] Typically, TEM pictures of each sample were taken: (i) at multiple, random locations in the sample (i.e., to ensure that the images reported are representative); (ii) at two different magnifications (100 and 430 K) in order to obtain information about the sample in general (100 K), plus a closer visualization of the clusters (430 K). A number of control experiments, done previously,[5b] provided good evidence that results of TEM visualizations obtained as described above are truly representative of the sample and that the sample is not perturbed by the TEM beam. For example, controls have been done: (i) showing that the TEM results did not change upon varying the sample spraying method (in air or under N_2) or when depositing the sample as a drop and letting it dry; and (ii) showing that the TEM images did not change when the beam voltage was changed from 40 to 100 kV, or if the exposure time was changed from seconds to minutes. Other controls have been done as well, and were reported previously.[5b]

Results and Discussion

(A) The Living-Metal Polymer Concept. In a fashion very similar to the well-known organic "living polymers",[7] previously isolated $Ir(0)_n$ clusters can serve as "seeds"[9] for further nanocluster growth. However, if isolated $Ir(0)_n$ clusters are to be used as seeds, then the Ir(0) autocatalytic growth by the reduction of precatalyst **1** to Ir(0) on the catalyst surface (step 4, Scheme 1; also eq 1b in the text) must prevail over any new nanocluster nucleation (steps 1−3, Scheme 1; also eq 1a in the text). This point can be understood by examining the relative rates of growth and nucleation, defined as R via eq 4.

$$R = \frac{\text{growth rate}}{\text{nucleation rate}} = \frac{k_2[\mathrm{A}][\mathrm{B}]}{k_1[\mathrm{A}]} = \frac{k_2[\mathrm{B}]}{k_1} \quad (4)$$

The ratio R under our standard conditions was estimated to be R = ca. 600 as computed from the following values:[16] $k_1 = 1.8 \times 10^{-3}$ h^{-1} and $k_2 = 1.8 \times 10^3$ M^{-1} h^{-1}, (see Figure 5a); $[\mathrm{B}]_{\mathrm{final}} = 0.5$ (1.2×10^{-3} M), vide infra. It is important to realize that for seed growth to occur *exclusively*, nucleation must be quenched *completely*, for as soon as nuclei are formed, growth will begin to take place on their surface.

In the following seed-growth experiments, $Ir(0)_{\sim 300}$ nanoclusters prepared under our standard conditions have been used as initial seeds of concentration $[\mathrm{B}]_0$. The seed-growth steps are then performed in the absence of cyclohexene, since the olefin would otherwise be in competition with the precatalyst for the catalyst surface.[17] The initial concentration of **1**, $[\mathrm{A}]_0$, and other conditions employed are essentially those stated as our standard conditions.

(13) Press: W. H.; Flannery, B. P.; Teukolsky, S. A.; Vetterling, W. T. *Numerical Recipes*; Cambridge University: Cambridge, 1989.

(14) (a) One sets[14b] $\Delta n(\mathrm{H_2})_{\mathrm{solution}} = \Delta n(\mathrm{H_2})_{\mathrm{gas}}$ where $\Delta n(\mathrm{H_2})_{\mathrm{gas}} = \Delta P(\mathrm{H_2})V_{\mathrm{gas}}/RT$, so that $\Delta[\mathrm{H_2}] = (\Delta P(\mathrm{H_2})V_{\mathrm{gas}})/(RTV_{\mathrm{solution}})$. (b) Lyon, D. K. Ph.D. Dissertation, University of Oregon, 1990. (c) We have $\Delta n(\mathrm{cyclohexene}) = \Delta n(\mathrm{H_2})_{\mathrm{solution}}$. For our apparatus, $V_{\mathrm{gas}} = 97$ mL and $V_{\mathrm{solution}} = 3$ mL, so that at $T = 22$ °C we have $\Delta[\mathrm{cyclohexene}]_{\mathrm{M}} = 0.0909\Delta P(\mathrm{H_2})_{\mathrm{psi}}$.

(15) Late in the reaction the cyclohexene concentration approaches zero, and hence the kinetics of the cyclohexene hydrogenation reaction (eq 1c) are no longer sufficiently fast, so that the cyclohexene hydrogenation reaction now also affects the observed kinetics, rather than serving as a pseudoelementary, "reporter" reaction.[4b]

(16) (a) The k_1 value is obtained by curve−fitting, $k_{1(\mathrm{fit})}$.[16d] (b) The k_2 value employed is that obtained from the curve−fit, $k_{2(\mathrm{fit})}$, but then adjusted by the mathematically required "stoichiometry factor" detailed elsewhere[4b] that is a consequence of using a pseudoelementary step and the olefin hydrogenation to follow the nanocluster formation.[16d] (c) No attempt was made, for the present semiquantitative studies, to also correct the $k_{2(\mathrm{fit})}$ by the "scaling factor" discussed elsewhere.[4b] (d) In the pseudoelementary model we follow the sum reaction (1d) by following $-\mathrm{d[cyclohexene]}/\mathrm{d}t$; since the sum reaction has the kinetics of the slow steps (1a−b), we fit $-\mathrm{d[cyclohexene]}/\mathrm{d}t$ to (eq 2): $-\mathrm{d[A]}/\mathrm{d}t = k_1[\mathrm{A}] + k_2[\mathrm{A}]([\mathrm{A}]_0 - [\mathrm{A}])$. That is, we curve-fit the following equation (eq 5): $-\mathrm{d[cyclohexene]}/\mathrm{d}t = k_{1(\mathrm{fit})}[\mathrm{cyclohexene}] + k_{2(\mathrm{fit})}[\mathrm{cyclohexene}]([\mathrm{cyclohexene}]_0 - [\mathrm{cyclohexene}])$. The stoichiometry of the sum reaction is such that: $\mathrm{d[cyclohexene]}/\mathrm{d}t \sim 1400\ \mathrm{d[A]}/\mathrm{d}t$ and $[\mathrm{cyclohexene}]_0 \sim 1400\ [\mathrm{A}]_0$, so that if we compare eq 2 and eq 5, we find that $k_1 = k_{1(\mathrm{fit})}$ while $k_2 \sim 1400\ k_{2(\mathrm{fit})}$ (where ~1400 is the exact ratio of $[\mathrm{cyclohexene}]_0/[\mathbf{1}]_0$ denoted as the "stoichiometry factor" [4b,16b]).

(17) There is an effect of cyclohexene on cluster growth, since the presence vs the absence of cyclohexene is the main difference in whether one obtains, respectively, the $Ir(0)_{\sim 300}$ vs $Ir(0)_{\sim 900}$ nanoclusters.[5b] The effect of cyclohexene is not fully understood and, hence, is still under investigation.

Effect of Initial "Seed" Concentration. The Example of an Initial Experiment That Failed. In the initial stages of the seed-growth process, eq 4 will hold true only if sufficient $[B]_0$ is present, that is, only if there are sufficient catalytic sites available on the $Ir(0)_n$ clusters' surface for precatalyst **1** to be reduced by the surface-autocatalytic pathway.[18] Experimental support for this point, and evidence that this translates to $[B]_0 \geq [A]_0$ for the present example, is illustrated by the failed experiment depicted in Figure 3b. First, however, Figure 3(a) shows the distribution of cluster sizes in a typical seed sample; the average nanocluster initial size is 21 ± 4 Å, within experimental error of the 20 ± 3 Å seen previously,[4,5] the approximately near-monodisperse[4e] *distribution* of Ir(0) nanoclusters defined[5] as $Ir(0)_{\sim 300}$. Figure 3(b) shows the distribution of cluster sizes found after an early *attempted* seed-growth step using these isolated $Ir(0)_{\sim 300}$ clusters and with an excess of $[A_0]$.[19] The histogram of cluster sizes *shows two maxima*, at 22 and 29 Å, suggesting that the cluster sizes are distributed around two average values. These maxima correspond, respectively, and within experimental error, to 20 Å or $Ir(0)_{\sim 300}$ clusters and 30 Å or $Ir(0)_{\sim 900}$ clusters. Since we know that, in the absence of cyclohexene (i.e., the conditions used in this experiment) and with the appropriate amount of **1** precursor present, $Ir(0)_{\sim 900}$ clusters are obtained,[5b,17] it follows that the observation of $Ir(0)_{\sim 300}$ clusters as well as $Ir(0)_{\sim 900}$ clusters as products is the result of our failure, in this initial experiment, to control (i.e., to stop) any new nucleation events. In this *unsuccessful* attempt, the relative concentrations of $Ir(0)_{\sim 300}$ and **1** were such that[19] $[B]_0 < [A]_0$ (specifically, $[B]_0 \sim [A]_0/8$). In the successful step II procedure which is described next, vide infra, the ratio is $[B]_0 \sim [A]_0$.

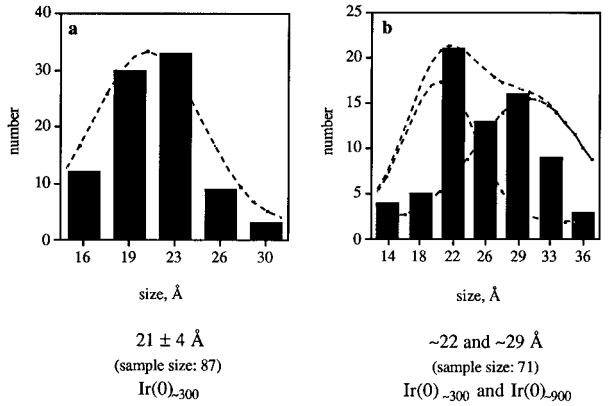

Figure 3. Histograms of $Ir(0)_n$ cluster sizes obtained: (a) under standard conditions; (b) after an unsuccessful seed-growth experiment due to the fact that $[B]_0 < [A]_0$ (specifically, $[B]_0 \sim [A]_0/8$). The TEMs from which the histograms shown were obtained are available as Figures A and B, Supporting Information.

Stoichiometric Seed-Growth Steps. Figure 4a shows the distribution of cluster sizes in a fresh $Ir(0)_{\sim 300}$ seed sample; the average cluster size is again 21 ± 4 Å and thus within experimental error of the expected 20 Å. Figure 4b shows the distribution of cluster sizes obtained after *two consecutive* seed-growth steps on these $Ir(0)_{\sim 300}$ nanoclusters (i.e., after Steps II plus III) and, again, where $[B]_0 \geq [A]_0$. As predicted, the observed cluster size of 26 ± 6 Å centers about 25 Å, that is, around $Ir(0)_{\sim 560}$ within experimental error. Figure 4c shows the distribution of cluster sizes obtained after another two consecutive seed-growth steps on the $Ir(0)_{\sim 560}$ clusters (i.e., after steps IV plus V). The average cluster size is 30 ± 5 Å, which now centers about 30 Å, or $Ir(0)_{\sim 900}$. While the observed TEM error bars of ±5 Å do not allow one to rigorously support the difference between the 25 Å and either the 20 or 30 Å nanoclusters, and although high-resolution (HR)-TEM data would of course be of value, there is a clear difference in size between the 20 and the 30 Å nanoclusters. And, in each case the *more reliable average or maximum*[20] of the distribution is right at the predicted three magic-numbers sizes, 20, 25, and 30 Å, corresponding to nanocluster distributions centering about $Ir(0)_{\sim 300}$, $Ir(0)_{\sim 560}$, and $Ir(0)_{\sim 900}$. In short, the trends and the *concept* are clear, and semiquantitatively so, even with the present, normal resolution (±2 Å) TEM data and resultant, overall ±5 Å error bars.

Referring back to Figure 2, it summarizes the values for $[A]_0$ (i.e., **1**) and $[B]_0$ (the $Ir(0)_n$ surface atoms, taken to equal the surface-active sites) in the experimentally executed sequence of seed-growth steps.[21a] These $[A]_0$ and $[B]_0$ data illustrate that *if* the relative concentrations of $Ir(0)_n$ and **1** in a seed-growth step are such that $[B]_0 \geq [A]_0$, *then* seed-growth on isolated $Ir(0)_n$ clusters is indeed successful. The sequence summarized in Figure 2 demonstrates that transition-metal nanocluster growth under H_2 can be accomplished in a predictable, stoichiometric manner.

The key finding, then, is that these $Ir(0)_n$ nanoclusters truly behave as "living metal polymers". A second major finding is that this mechanism-based insight[4b] can, in turn, be exploited to give—*by design*—a series of nanoclusters that center about prechosen, magic-number sizes.

(B) Prediction, then Experimental Demonstration, of $Ir(0)_n$ Nanocluster Size Control Using the

(18) It is important to note that one batch of $Ir(0)_{\sim 300}$ clusters prepared under standard conditions provides $[B]_{final} \sim ([A]_0/310)160 \sim ([A]_0/2)$ (310 is the total number of atoms; 160 is the number of surface atoms in a $Ir(0)_{\sim 300}$ cluster).[26a] Hence, if only one of these batches is used for seed growth with the precatalyst **1** at its standard conditions concentration (1.2 mM), then one will have $[B]_0 \sim ([A]_0/2)$.

(19) The specific conditions were: $[Ir(0)_{\sim 300}] \sim 10^{-3}$ mM and $[B]_0 \sim 0.16$ mM, $[\mathbf{1}] = [A]_0 = 1.2$ mM, and no cyclohexene.

(20) (a) Note that it is crucial in examining any of the TEM histograms to realize that a comparison of the average value or maximum seen in the histograms should be more reliable since any *systematic* errors will tend to cancel. Note also that one should focus on the shape and maximia of the histograms since the widths of the black bars used in such histograms are ca. 2 Å and thus less than the experimental error of ca. ±5 Å that arises as a combination of the errors in: (i) the TEMs ±2 Å inherent resolution, (ii) the print magnification of the TEM negative that is used to count the different size nanoclusters, and (iii) the finite precision of the subdivisions of the ruler used by eye to count the nanocluster sizes. (b) A referee has noted, and we agree, that "what is really lacking in the whole area (worldwide) is a reliable and standardized way to evaluate TEM grids" (i.e., in terms of how may portions of the grid, the number of particles that minimally should be counted, and so on). We worried here (and previously; see our original TEM Experimental section on p 8348 elsewhere[5b]) about these important issues. This is one reason we carefully cite herein our TEM sampling methods, our multiple TEM control experiments (see Experimental Section) and also why we cite the number of particles counted with each TEM and its associated histogram.

(21) (a) $[Ir(0)_n]_{(\text{step } X)} = ([A]_{0(\text{step } X)})/n$ and $[B]_{0(\text{step } X+1)} = [Ir(0)_n]_{(\text{step } X)} \times$ (number of surface atoms). For example, the fact that the $Ir(0)_n$ average cluster size between steps I and III changes from 300 to 550 atoms can be accounted for as follows: $310(n \text{ per cluster})_{\text{step I}} + 150([A]_0 \text{ per cluster})_{\text{step II}} + 100([A]_0 \text{ per cluster})_{\text{step III}} = 500(n \text{ per cluster})_{\text{step III}}$. (b) Rigorously, the quantity $[B]_t$ is a function of cluster size. This follows since the number of *surface* atoms [B] in a given $Ir(0)_n$ sample is inversely dependent on the cluster size, n.

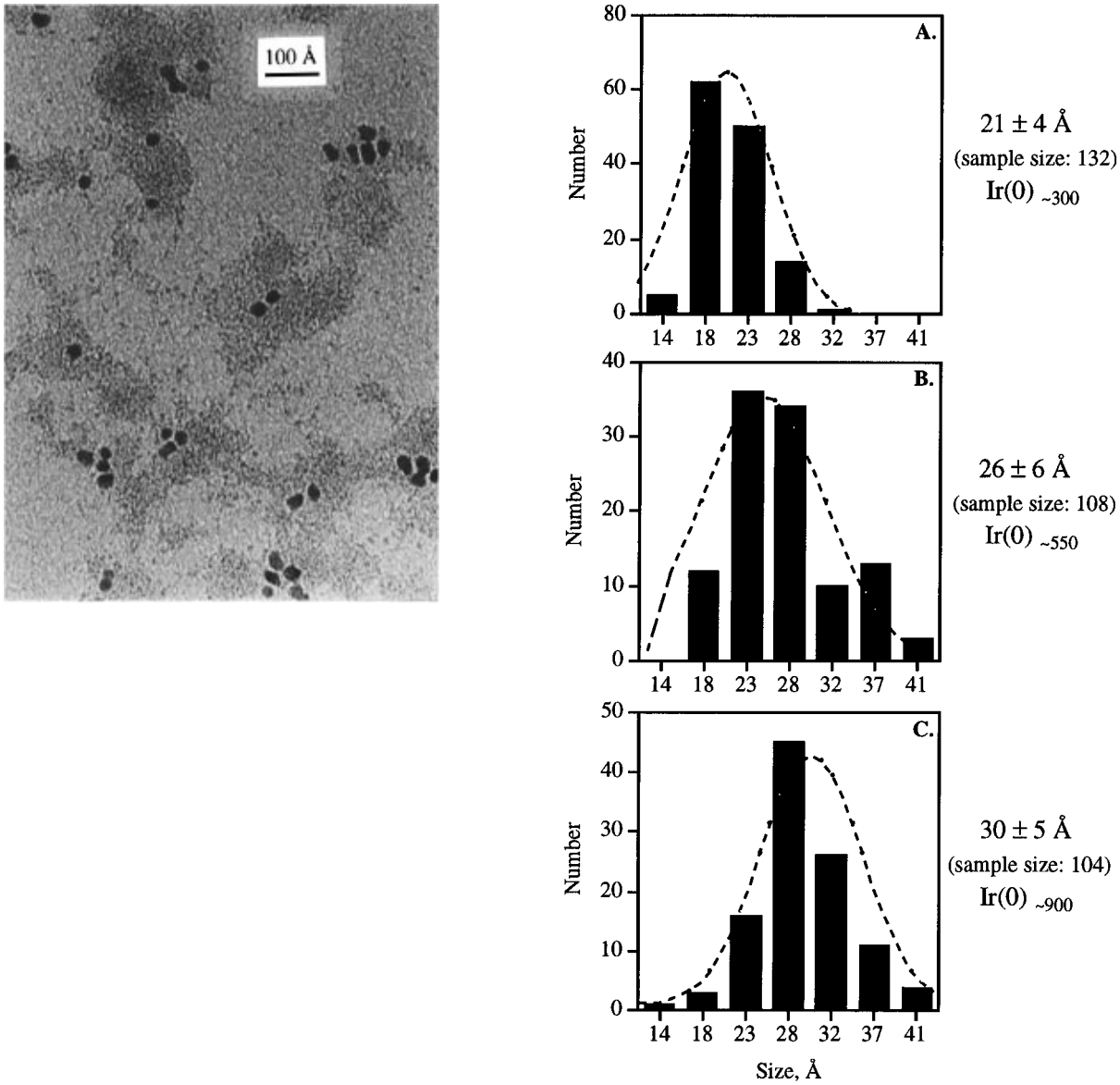

Figure 4. TEM of $Ir(0)_{\sim 300}$ nanoclusters prepared as in the step I standard conditions, and histograms of $Ir(0)_n$ cluster sizes obtained: (a) under standard conditions, step I; (b) after seed-growth steps II plus III; and (c) after seed-growth steps IV plus V. TEMs from which the histograms in (b) and (c) were obtained are available as Figures C and D of the Supporting Information. Note that, in these and all the other histograms presented as part of this work, it is the indicated *average size* which is more reliable than the apparent histogram maxima in identifying the desired, true center of the distribution. This is true because the width of the histogram's black bars is less than the ca. ±5 Å experimental uncertainty; hence, focusing on the highest bar rather then the more telling shape of the histogram can be misleading.[20] For this reason, we've added dotted lines to the histograms showing their basic shape and indicating the approximate maximum (or maxima) of each distribution.

Ratio of Rate Constants, $R' = k_2/k_1$. The relative rates of growth, eq 1b, and nucleation, eq 1a, during $Ir(0)_n$ nanocluster formation determine the final $Ir(0)_n$ cluster size as indicated by the ratio $R = k_2[B]_t/k_1$ (recall eq 4). However, since the quantity $[B]_t$ is not easily estimated,[21b] we explored the following approximate—but, as it turns out, useful—way to proceed. If we assume that $[B]_t$ is constant throughout the comparisons that follow, then we can consider the ratio of *rate constants*, $R' = k_2/k_1$ (M^{-1}). As before with the ratio of rates, R, the ratio of rate constants, R', can also then be used to *predict* $Ir(0)_n$ nanocluster sizes obtained under different experimental conditions (different R' ratios): the formation of larger $Ir(0)_n$ nanoclusters is expected for larger R' values, while the formation of smaller $Ir(0)_n$ nanoclusters is expected for smaller R' values. Experimentally, the rate constants k_2 and k_1 were obtained as before, from curve-fitting the hydrogen (or cyclohexene[22]) loss vs time data.[4b] Note that one need *not* correct the R' by the "scaling" correction factors that we detailed previously[4b] (although the $k_{2(fit)}$ is, as a matter of consistency, always corrected by the previously discussed "stoichiometry factors").[16]

(i) Standard Conditions. Figure 5a shows a curve-fit of the cyclohexene loss monitored under standard conditions. The induction period is $t_{(induction)} = 1.55$ h, and the cyclohexene hydrogenation rate is $-d[H_2]/dt = 2.7$ mmol/h. The calculated ratio of rate constants under the standard conditions of this experiment is $R'_{standard} = 1.0 \times 10^6$ M^{-1}. As already demonstrated via both Figure 5b and, equivalently, Figure 4a, the average

(22) Note that the cyclohexene is 1.65 M, while the $Ir(0)_n$ nanoclusters are produced in catalytic amounts, $[Ir]_{total} = 1.2$ mM. Hence, when we follow the net reaction, eq 1d, we are following H_2 consumption that corresponds (to within 1 part in 10^3) to only the cyclohexene reduction, eq 1c.[4b]

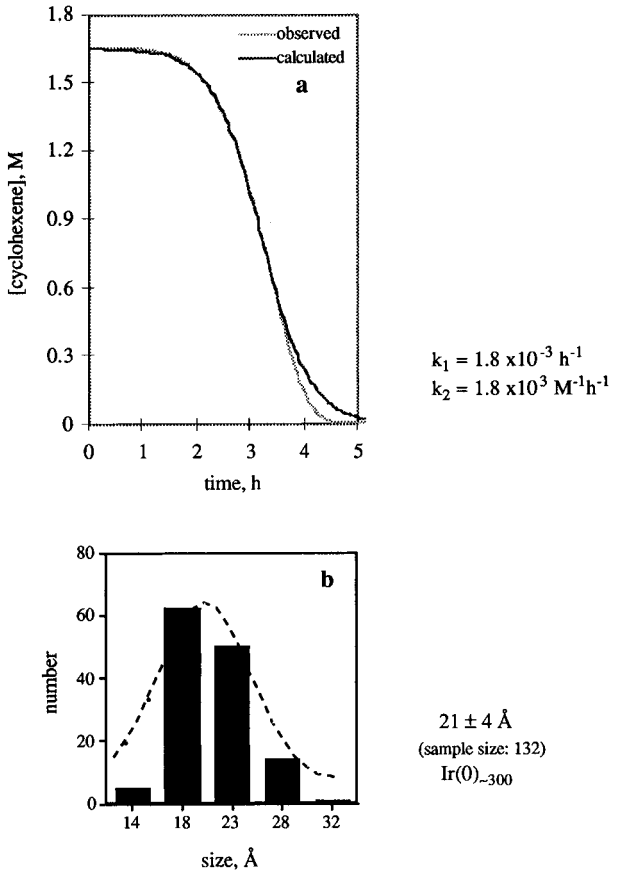

Figure 5. Ir(0)$_n$ clusters prepared under standard conditions: (a) curve-fit of cyclohexene uptake; (b) histogram of the resultant nanocluster size distribution. The TEM from which this histogram was obtained is available in Figure 4.

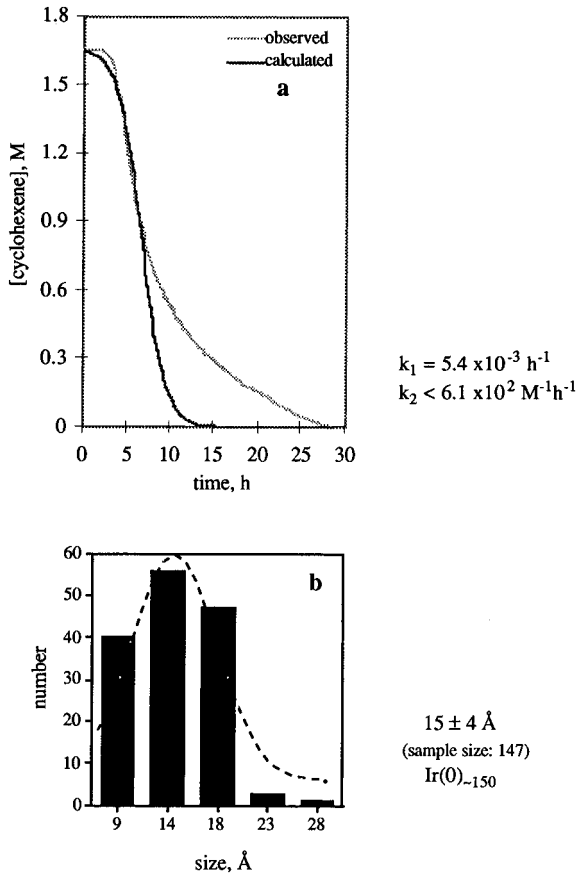

Figure 6. Ir(0)$_n$ clusters prepared in the presence of 7.5 equiv of added polyoxoanion: (a) curve-fit of cyclohexene uptake; (b) histogram of the resultant nanocluster size distribution. The TEM from which this histograms was obtained is available as Figure E of the Supporting Information.

nanocluster size corresponding to this $R'_{\text{standard}} = 1.0 \times 10^6$ M^{-1} is 21 ± 4 Å, a distribution which centers about ca. 20 Å or Ir(0)$_{\sim 300}$.

(ii) The Effect of Added Excess Polyoxoanion. At this point we simply scanned the many other nanocluster formation reactions that we had run under a variety of conditions[4,5] to find one whose R' value was significantly smaller so that smaller nanoclusters were predicted to be present. Figure 6a shows just such a system: a curve-fit of the cyclohexene uptake monitored in the presence of 7.5 added equivalents (vs precatalyst **1**) of the polyoxoanion $(Bu_4N)_9[P_2W_{15}Nb_3O_{62}]$, **2**. The induction period and rate for cyclohexene hydrogenation in this run are $t_{\text{induction}} = 3.2$ h and $-\text{d}[H_2]/\text{d}t = 0.9 \pm 0.4$ mmol/h, respectively.[23] In addition, the fact that the observed cyclohexene uptake curve deviates from a symmetrical "S" shape that is typical for autocatalysis,[4b] together with the observation that the rates of cyclohexene hydrogenation are not reproducible within the usual ±10% range,[4b,5a] strongly suggests that the presence of a large excess of polyoxoanion "blocks" the Ir(0)$_n$ catalyst surface, thereby decreasing k_2. The estimated rate constant ratio when 7.5 equiv of polyoxoanion/equiv **1** is present is $R'_{\text{polyoxoanion}} \sim 4.5 \times 10^4$ M^{-1}.[24] This in turn allows one to calculate $R'_{\text{polyoxoanion}} \sim (1/20) \times [R'_{\text{standard}}]$ from which one predicts that the desired, *smaller* Ir(0)$_n$ nanoclusters (i.e., smaller than the Ir(0)$_{\sim 300}$ formed under standard conditions) should form under these excess polyoxoanion conditions.

Figure 6b shows the distribution of cluster sizes actually obtained in the presence of 7.5 added equivalents of polyoxoanion. The average cluster size is indeed 15 ± 4 Å, which centers about 15 Å, or Ir(0)$_{\sim 150}$, within experimental error, close to the next smaller magic number, Ir(0)$_{147}$. This experiment illustrates a remarkable amount of prediction, control, and, ultimately, mechanistic understanding[4b] in an area where there was previously almost none.

(iii) Small Effect of the 18 °C Lower Temperature (3 °C). The temperature dependence of the $R' = k_2/k_1$ ratio is another way to control nanocluster size, at least in principle and depending, of course, on the particular system at hand. For the present polyoxoanion-supported organometallic nanocluster precursor, **1** Figure 7a) shows a curve-fit of the cyclohexene uptake monitored at 3 °C rather than the 22 °C in the standard conditions. The induction period and rate for cyclohexene hydrogenation are now longer and smaller, respectively (i.e., a smaller k_1 and a smaller k_2) as generally

(23) (a) Both the induction period and the rate for cyclohexene hydrogenation are somewhat dependent upon the batch of polyoxoanion used (i.e., are sensitive to one's attention to detail and care in preparing the batch of polyoxoanion[12] used; see footnote 28 elsewhere[4b]). (b) Also, in the presence of a *large excess* of added polyoxoanion, the hydrogenation rate is less reproducible (spanning a ±50% range), as opposed to the usual ±≤15% range detailed elsewhere.[4b]

(24) Suspecting that the actual value for k_2 is somewhat smaller than the calculated one, that is, given the relatively poor curve-fit exhibited in Figure 6a, and since the observed uptake of cyclohexene is about 2−3 times slower than the calculated one (see Figure 6a), we have estimated k_2 as $k_{2(\text{estimated})} \sim (k_{2(\text{fit})}/2.5)$.

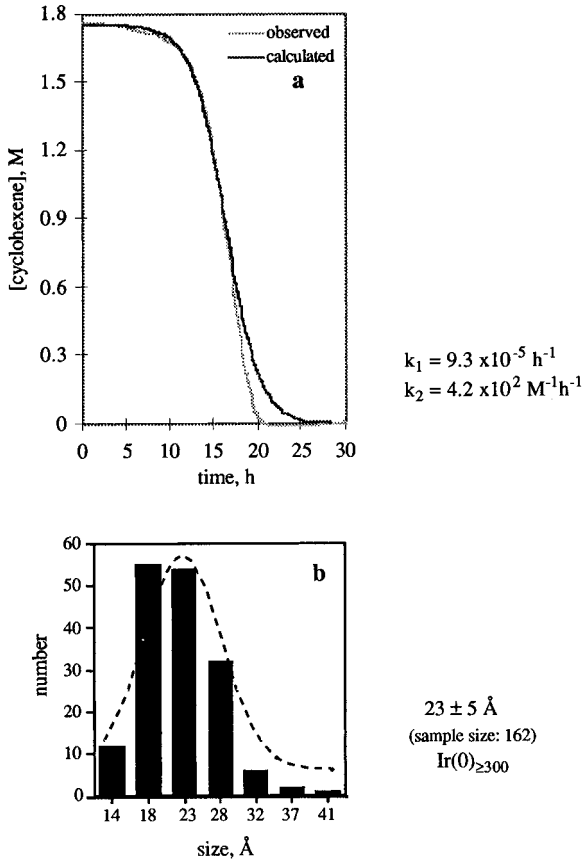

Figure 7. Ir(0)$_n$ clusters prepared at lower, 3 °C temperature: (a) curve-fit of cyclohexene uptake; (b) histogram of the resultant nanocluster size distribution. The TEM from which this histogram was obtained is available as Figure F of the Supporting Information.

expected for lower temperature, $t_{\text{induction}} = 12.4$ h, and $-\text{d}[\text{H}_2]/\text{d}t = 0.9$ mmol/h, respectively. The calculated rate constants k_2 and k_1 give the ratio at 3 °C of $R'_{3\,°\text{C}} = 4.5 \times 10^6$ M^{-1}. The computed relative ratio is $R'_{3\,°\text{C}} = 4.5\ R'_{\text{standard}}$, and thus *some* tendency toward *larger* Ir(0)$_n$ clusters is expected for at least this system and its 18 °C lower temperature. However, since the previous experiment with a 7.5 equiv excess of polyoxoanion and which exhibited a relative R' ratio of ca. 20 showed a difference in average cluster size of only ca. 5 Å (or one Ir(0)$_n$ atomic shell[5b]), one can anticipate that any size difference will likely be less than our TEM detection limit of ±5 Å.

Figure 7b shows the experimental results, specifically the distribution of cluster sizes obtained for the 3 °C synthesis. The average cluster size of 23 ± 5 Å is, as anticipated, only an *apparent* 2 Å larger than (and, rigorously, not different statistically within experimental error of) the 21 ± 4 Å nanoclusters formed under the 22 °C of our standard conditions. Hence, we will label these clusters as Ir(0)$_{\geq 300}$, consistent with the lack of a non-HR-TEM detectable size change.[25] Even this result is, however, quite intriguing in that it suggests a useful goal of future research is to obtain an experimental R' ratio vs HR-TEM observed size curve: what does the curve look like and just how sensitive is the R' function as a predictor of size changes (i.e., in comparison to the powerful but slow technique of HR-TEM)? The needed studies of both good statistics *and* independent size confirmation by, for example, a combination of HPLC and HR-TEM, are the basis of a separate project.

A Mechanism-Based Explanation for the Formation of "Magic-Number" Size Transition-Metal Nanoclusters: Autocatalytic *Surface Growth*. One of the intriguing phenomena in nanocluster science[1] is the observation of so-called "magic-number" clusters, that is, full-shell clusters that are of enhanced stability.[26] In the case of transition metals (M),[27] magic-number clusters contain M_{13}, M_{55}, M_{147}, M_{309}, M_{561}, M_{923}, or M_{1415} (and so on) metal atoms, where the number of surface atoms in the nth shell is given by $10n^2 + 2$. This formula holds true regardless of whether the structure is cuboctahedral (ccp or, equivalently, fcc) or twinned cuboctahedral (hcp).[26a] Note that such transition-metal nanocluster formation must be under *kinetic control*, since it is easily demonstrated that a typical transition-metal nanocluster is higher in energy than the thermodynamic sink of bulk metal formation.[28] It was striking to us in our initial ca. 1990 discovery and synthesis of Ir(0)$_{\sim 300}$ and Ir(0)$_{\sim 900}$ nanoclusters that, *without trying*, we had prepared a distribution of nanoclusters centering around the M_{309} (i.e., Ir(0)$_{\sim 300}$) and M_{923} (i.e., Ir(0)$_{\sim 900}$) magic numbers. The available nanocluster or nanocolloid literature[1,26] was unable to provide any *mechanistic* insight into *why or how* magic-number nanoclusters had tended to form, so this

(25) It is worth noting that our recent study found equivalent enthalpies within experimental error for the composite steps represented by k_1 and k_2 ($\Delta H_1^{\ddagger} = 15 \pm 1$ kcal/mol and $\Delta H_2^{\ddagger} = 14 \pm 2$ kcal/mol).[4b] Hence, those results independently predict the small dependence of size upon temperature confirmed as part of the present study.

(26) Lead references to the concept of "magic number" clusters: (a) Teo, B. K.; Sloane, N. J. A. *Inorg. Chem.* **1985**, *24*, 4545. (b) Wells, A. F. *Structural Inorganic Chemistry*, 4th ed.; Clarendon Press: Oxford, 1975. Pages 123 and 131 provide a concise discussion of sphere packings and their relationships to the 12 nearest-neighbor atoms that define cubooctahedral (ccp, or equivalently, fcc) and twinned cubooctahedral (hcp) discrete structures. (c) Howie, A. *Faraday Discuss.* **1991**, *92*, 1 (see pp 2−3). (d) Klots, T. D.; Winter, B. J.; Parks, E. K.; Riley, S. J. *J. Chem. Phys.* **1990**, *92*, 2110.

(27) (a) The transition-metal magic numbers should not be confused with the earlier, better characterized, and first true magic number clusters of a different type based on the alkali metals: M_n (M = Na, K, Cs), where n = 2, 8, 20, 40, 58, 92, 138, and so on). For a good discussion of the difference of these magic numbers from those based on icosahedral or cubo−octahedral structures, see elsewhere.[26c] (b) Other workers have reported a structured size distribution that consists of "magic *agglomeration* numbers" of $(CdS)_{8n}$ nanoclusters.[27c] They suggest that such a distribution is the result of a large ratio of the rate of nucleation to growth, followed by agglomeration of the $(CdS)_8$ nuclei to give larger clusters. Thus, integral multiples of 8 are seen, but these semiconductor nanoparticles are, of course, neither the *alkali metal* magic number cluster sizes (M_n, where n = 2, 8, 20, 40, 58, 92, 138, and so on) nor are they the *transition-metal* magic number clusters (M_{13}, M_{55}, M_{147}, M_{309}, M_{561}, M_{923}, M_{1415}, and so on). That is, the interesting 1984 paper[27c] does not provide a mechanistic explanation for magic number nanoclusters of either of the two known classes. (c) Fojtik, A.; Weller, H.; Koch, U.; Henglein, A. *Ber. Bungen-Ges. Phys. Chem.* **1984**, *88*, 969. (d) Noteworty is Bawendi and co-workers' brief discussion, on p 8708, of magic number sizes in CdE (E = S, Se, Te) semiconductor particles in terms of a *thermodynamic* "bottleneck" that reduces the driving force for further growth. Murray, C. B.; Norris, D. J.; Bawendi, M. G. *J. Am. Chem. Soc.* **1993**, *115*, 8706. Note, however, that this brief statement is ambiguous in whether or not the production of CdE is ultimately *thermodynamically* or *kinetically* controlled.

(28) This can be seen by, for example, considering the case of bulk Ir(0) relevant to the present paper concerned with Ir(0) nanoclusters. The $\Delta H_{\text{vaporization}}$ of bulk Ir(0) metal is 159 kcal/mol (Porterfield, W. W. *Inorganic Chemistry*; Addison-Wesley Publishing: Reading, MA, 1983; p 84). This in turn means that 12-coordinate Ir(0) in the bulk solid experiences an average bond energy of 159/(12/2) = 26 kcal/mol (12/2 since it takes 2 Ir atoms to form 1 Ir−Ir bond). This back-of-the-envelope analysis[38b,c] reveals the driving force for Ir(0)$_x$ nanoparticles to aggregate to the thermodynamically favored, low-surface-area solid, thereby revealing that this and similar nanocluster syntheses are under kinetic control.

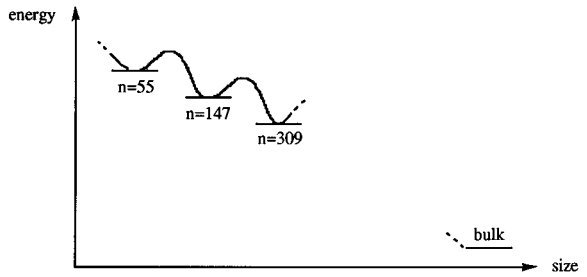

Figure 8. Schematic representation of the expected continuous decrease in energy as a function of nanocluster size to the limit of bulk metal. Local minima are shown at each closed shell, magic-number size (and thus extra stability) nanocluster.

important question has remained unanswered until now.

It is important before proceeding further to be aware of the four lines of established evidence[4a,b] which require that the autocatalytic growth step is *on the surface of the nanocluster*. That evidence is (i) the fact that transition metal catalysis invariably occurs *on the metal's surface*, for example, the activation of H_2 in the present example (i.e., the finding of autocatalysis itself), (ii) the fact that any isolated Ir(0) atoms produced in solution are considerably higher in energy than when bound to $Ir(0)_n$ as in $Ir(0)_{n+1}$ (i.e., roughly m·26 kcal/mol higher in energy, where m = the number of Ir(0)−Ir(0) bonds made upon forming $Ir(0)_{n+1}$ from $Ir(0)_n$, a number that is nominally ≥78 kcal/mol); (iii) the work presented herein providing evidence that the $Ir(0)_{\sim 300}$ nanoclusters behave as "living (metal) polymers" whose size can be increased simply by adding more [(1,5-COD)-Ir·$P_2W_{15}Nb_3O_{62}$]$^{8-}$ precursor, and (iv) evidence from the literature.[29] In short, the evidence presented originally elsewhere[4a,b] is compelling that the Ir(0) nanoclusters in the present paper are formed via an *autocatalytic surface-growth* mechanism.[4]

The establishment of an autocatalytic surface-growth mechanism allows us to offer the first mechanism-based explanation[27d] for a tendency to form magic-number nanoclusters under H_2 if we simply consider which nanoclusters will grow faster or slower, and why. Following generation of $Ir(0)_n$ nuclei of a small but critical size (n),[4a,b] surface autocatalytic growth commences. However, when a given cluster reaches a magic-number size, it attains the added thermodynamic stability associated with a full-shell number of metal atoms, an enhanced stability derived from the fact that each surface metal atom has the maximum number of metal−metal bonds,[26] (Figure 8). Hence it is somewhat more stable and will, therefore, *tend to grow more slowly*. On the other hand, non-magic-number nanoclusters will continue to grow rapidly. In other words, *magic numbers are the expected, natural consequence of surface autocatalytic growth*. Their observation in many nanocluster syntheses under H_2[4b,5,10a,b,30] is, in turn, consistent with and actually strong evidence for the greater generality[31] of the autocatalytic surface-growth mechanism (although it cannot, of course, extend to metals that are not reducible thermodynamically[32] by H_2[33]).

Finally, a noteworthy insight is that magic-number nanoclusters are actually anything but "magic" in that they should be both more common *and* somewhat less reactive as catalysts (albeit more stable and thus presumably longer-lived than non-magic-number size, nonnanocluster catalysts). A referee has suggested that they be called "closed-shell clusters" instead of magic number clusters, a good suggestion in our opinion. On *non*-magic-number (i.e., on *non*-closed-shell) nanoclusters, the presence of high-reactivity sites such as steps, kinks, and adatoms should further add to their greater reactivity in comparison to the more common, and therefore better studied, magic-number sized nanoparticle catalysts.

Living Metal−Polymer Based Predictions for the Rational Synthesis of Known Initial Structure, Bi- Tri-, and Higher Multimetallic Nanoclusters. There is one additional, important prediction of the autocatalytic surface-growth mechanism and its living metal-polymer phenomenon. That prediction, illustrated in Scheme 2, is that it should be possible to rationally design, then prepare, a complete series—at least in principle—of all possible "onionskin" structure

(29) Whitesides and co-workers have provided detailed studies of the Pt(0)-surface catalyzed growth of Pt(0) particles from Pt(1,5-COD)-R_2 (R = alkyl),[29a−d] work which provides some precedent for the Ir cluster growth step presented herein. However, compelling evidence for the autocatalytic nature of this key step has not been previously described. (a) McCarthy, T. J.; Shih, Y.-S.; Whitesides, G. M. *Proc. Natl. Acad. Sci. U.S.A.* **1981**, *78*, 4649. (b) Whitesides, G. M.; Hackett, M.; Brainard, R. L.; LaVelleye, J. P.-P.; Sowinski, A. F.; Izumi, A. N.; Moore, S. S.; Brown, D. W.; Staudt, E. M. *Organometallics* **1985**, *4*, 1819. (c) Miller, T. M.; Izumi, A. N.; Shih, Y.-S.; Whitesides, G. M. *J. Am. Chem. Soc.* **1988**, *110*, 3146. (d) Lee, T. R.; Whitesides, G. M. *Acc. Chem. Res.* **1992**, *25*, 266 and references therein to the other papers in this series.

(30) (a) G. Schmid, M. Harms, J.-O. Malm, J.-O. Bovin, J. Van Ruitenbeck, H. W. Zandbergen, W. T. Fu, *J. Am. Chem. Soc.* **1993**, *115*, 2046. (b) G. Schmid, V. Maihack, F. Lantermann, S. Peschel, *J. Chem. Soc., Dalton Trans.* **1996**, 589.

(31) (a) Ahmadi, T. S.; Wang, Z. L.; Henglein, A.; El-Sayed, M. A. *Chem. Mater.* **1996**, *8*, 1161. (b) Ahmadi, T. S.; Wang, Z. L.; Green, T. C.; Henglein, A.; El-Sayed, M. A. *Science* **1996**, *272*, 1924. (c) J. Kiwi, M. Grätzel, *J. Am. Chem. Soc.* **1979**, *101*, 7214. (d) Bönnemann, H.; Brinkmann, R.; Köppler, R.; Neiteler, P.; Richter, J. *Adv. Mater.* **1992**, *4*, 804. (e) Bönnemann, H.; Brijoux, W.; Brinkmann, R.; Fretze, R.; Joussen, T.; Köppler, R.; Korall, B.; Neiteler, P.; Richter, J. *J. Mol. Catal.* **1994**, *86*, 129. Reported therein is that Pd(0), formed initially from R_3BH^- reduction of Pd^{2+}, catalyzes further nanocluster growth by reducing—we'd guess autocatalytically—additional Pd^{2+} using H_2 (see p 155). (f) Review: Bönnemann, H.; Brijoux, W. In *Active Metals*; Fürstner, A. VCH Publishers: New York, 1996; Chapter 9, pp 339−397. Note on p 361 the use of H_2 as a preferred reducing agent. (g) Rampino, L. D.; Nord, F. F. *J. Am. Chem. Soc.* **1942**, *63*, 2745. (h) Henglein, A.; Ershov, B. G.; Malow, M. *J. Phys. Chem.* **1995**, *99*, 14129. (i) Toshima, N.; Takahashi, T. *Bull. Chem. Soc. Jpn.* **1992**, *65*, 400. (j) Boutonnet, M.; Kizling, J.; Stenius, P.; Maire, G. *Colloids Surfaces* **1982**, *5*, 209. (k) Harrison, J. B.; Berkheiser, V. E.; Erdos, G. W. *J. Catal.* **1988**, *112*, 126. (l) Yonezawa, T.; Tominaga, T.; Richard, D. *J. Chem. Soc., Dalton Trans.* **1996**, 783. (m) J. Blum, I. Amer, K. P. C. Vollhardt, H. Schwarz, G. Höhne, *J. Org. Chem.* **1987**, *52*, 2804.

(32) The interesting cases of magnetic nanoclusters of Co, Fe, and Ni are, unfortunately, almost never[33a] produced under H_2 since they are not reducible, thermodynamically speaking, by H_2[33b] at least under standard conditions ($E_{1/2}(Co^{2+}/Co^0) = -0.28$ V, $E_{1/2}(Fe^{2+}/Fe^0) = -0.41$ V, $E_{1/2}(Ni^{2+}/Ni^0) = -0.23$ V vs H_2).

(33) (a) Nanoclusters of Co have been prepared by H_2 reduction of an organometallic precursor, but the reduction was, apparently, that of the attached ligand: Osuna, J.; de Caro, D.; Amiens, C.; Chaudret, B.; Snoeck, E.; Respaud, M.; Broto, J.−M.; Fert, A. *J. Phys. Chem.* **1996**, *100*, 14571. (b) Bard, A. J.; Faulkner, L. R. *Electrochemical Methods: Fundamentals and Applications*; Wiley-Interscience: New York, 1980. (c) Gibson, C. P.; Putzer, K. J. *Science* **1995**, *267*, 1338. (d) Hess, P. H.; Parker, P. H. *J. Appl. Polym. Sci.* **1966**, *10*, 1915. (e) Billas, I. M. L.; Châtelain, A.; de Heer, W. A. *Science* **1994**, *265*, 1682. (f) Gong, W.; Li, H.; Zhao, Z.; Chen, J. *J. Appl. Phys.* **1991**, *69*, 5119. (g) Yiping, L.; Hadjipanayis, G. C.; Sorensen, C. M.; Klabunde, K. J. *J. Appl. Phys.* **1990**, *67*, 4502. (h) Che, J.−P.; Sorensen, C. M.; Klabunde, K. J.; Hadjipanayis, G. C. *J. Appl. Phys.* **1994**, *76*, 6316. (i) Becker, J. A.; Schäfer, R.; Festag, R.; Ruland, W.; Wendroff, J. H.; Pebler, J.; Quaiser, S. A.; Helbig, W.; Reetz, M. T. *J. Chem. Phys.* **1995**, *103*, 2520. (c) Sonochemical synthesis of Fe nanoclusters from Fe-$(CO)_5$: Suslick, K. S.; Fang, M.; Hyeon, T. *J. Am. Chem. Soc.* **1996**, *118*, 11960.

Scheme 2. Illustration of the Living Metal−Polymer Approach to the Synthesis of Multimetallic Nanoclusters of, at Least in Principle,[a] Well-Defined Initial Structure and Layer Thickness. The Specific Example Shown Illustrates the Synthesis of All Possible Geometric Isomers of a Trimetallic Nanocluster

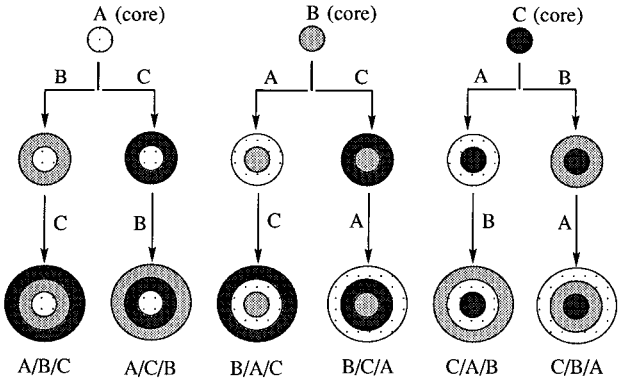

[a] It needs to be emphasized that this scheme *is idealized* and intended only to illustrate the concept involved. It is already known for example, that some bimetallic nanoclusters do *not* show such idealized second layers as illustrated above.[35,36a] In addition, if a lattice or symmetry mismatch exists between the layers, thereby creating a high interfacial energy, it is more likely that imperfect (e.g., mound or island) growth will occur (e.g., as seen in molecular-beam epitaxial growth).[35c] Layer (atomic) migrations can also occur.[36a] However, it is also likely that closer to idealized bi- and higher multimetallic nanoclusters can be obtained by application of the autocatalytic surface-growth mechanism and the other principles provided by the present study.

geometric isomers of bi-, tri-, and higher multimetallic nanoclusters.[34] Note that one needs (i) the desired seed or central core nanocluster, (ii) a predetermined amount of metal precursor for each additional, prechosen shell thickness, and, of course, (iii) each metal must be reducible by hydrogen since this is the only reductant, at least presently, for which the autocatalytic surface-growth mechanism is firmly established.[4b] In addition (iv) the core metal, and then each added layer, must be able to *activate* H_2 (i.e., and not just be thermodynamically reducible by H_2), and (v) the reaction conditions must not permit separate nucleation of the metal added for the next layer.[35a,b] Note also that a key advantage, again at least in principle, is that each geometric isomer in Scheme 2 is of known *initial* structure. Layer (atomic) migration phenomenon[36a] are known, however, and will mitigate against the idealized structures in Scheme 2.

However, the conceptual significance of Scheme 2 to nanocluster science can be seen by analogy to the significance, in the pre-NMR days of organic chemistry, of independent synthesis via established reactions as a key method of *structure proof*. That is, the use of synthesis to produce known structures is exceedingly valuable in any area where independent proof of structure is difficult, as it is for multimetallic composition nanoclusters. The important difference in this organic chemistry vs metal nanocluster analogy is, however, that the kinetic mobility of the initial metal core vs the initial outer metal layer(s) should be much higher in the case of metals (i.e., vs the static C−C bonds of covalent organic compounds).

Worth noting is that the availability of onionskinned initial structure multimetallic nanoclusters, such as those in Scheme 2, will open to investigation some fundamental issues and other interesting questions, for example: (i) the catalytic[36] and other materials properties of the bi-,[37] tri-, and higher multimetallic nanoclusters of *known initial structure* and (ii) fundamental structural issues such as which metal will prefer the core vs the surface of the nanocluster and why (i.e., which structure is the thermodynamic minimum, and which structures are only kinetically stable?).[38] Alternatively, (iii) which systems prefer, instead, to make alloyed structures *at the nanoscopic level*?[39] In fact, the seeded autocatalytic surface-growth principle has already been used by Schmid and co-workers to make bimetallic nanoclusters.[9a] But, a survey of the growing literature of bi-metallic nanoclusters formed under H_2 reveals that *the principle illustrated in Scheme 2 is little*

(34) (a) Professor Schmid and co-workers recent contribution to the bimetallic nanocluster area illustrates both some of the exciting prospects, and also some of the issues which require investigation, in the living-metal−polymer (i.e., seed growth) synthesis strategy and in the use of the resultant materials in catalysis.[36a] These workers prepared Au(core)/Pt and Pd(core)/Pt nanoclusters, as well as the monometallic Au and Pt nanoclusters as controls, and these particles were each separately supported on Al_2O_3 and then tested for their hydrosilation catalysis activity. The interesting finding is than the Pd/Pt catalyst is ca. 3-fold more active that the Au/Pt catalyst, with the Pd and Au nanoclusters proving inactive. One main issue here, however, is that the rates are not corrected for the exposed surface area, something that has long been known to be crucial in heterogeneous catalysis.[34b] Also of interest is the observation by TEM that the Pt surface layer of both the Au and Pd core nanoclusters is much less uniform than the idealized representation in Scheme 2 nominally imply. Note, however, that the observed, "noncontiguous layer of Pt" but, instead, "Pt particles of ca. 5 nm...probably formed in a separate nucleation process"[36a] is *exactly* what our autocatalytic surface-growth mechanism predicts for Au(core)/Pt, *since Au is known to be a slow hydrogenation catalyst relative to metals such as Pt*.[34c] The reason the Pt surface of the Pd(core)/Pt nanoclusters is less uniform is not clear, and a difficult issue here is whether or not the Pd and Pt have begun to exchange positions (i.e., with some surface Pd) as one expects thermodynamically.[38] We note, however, that none of these issues—ones expected given the early state of bimetallic nanocluster chemistry—detracts whatsoever form the significance of Professor Schmid's important early contribution or from the exciting prospects their work foretells. (b) Boudart, M.; Dje'ga-Mariadassou, G. *Kinetics of Heterogeneous Catalytic Reactions*; Princeton University Press: Princeton, NJ, 1984. (c) Naito, S.; Tanimoto, M. *J. Chem. Soc. Chem. Commun.* **1988**, 832 and refs 1−3 therein.

(35) (a) Au core nanoclusters should be a classic case where these conditions are *not* met, and the TEM of recently reported Au(core)/Pt nanoclusters confirms these expectations.[36a] (b) See the TEM in Figure 2 elsewhere showing "Ag staining" of Pt nanoclusters (i.e., Ag growth on Pt nucleation sites; Figure 2). Ketelson, H. M.; Brook, M. A.; Pelto, R.; Heng, Y. M. *Chem. Mater.* **1996**, *8*, 2195; see also refs 26 and 27 therein to Cu, Ni and other metal deposition on, for example, preformed Pd and Pt colloids. (c) Vidali, G. in *Nanoparticles in Solids and Solutions*; Fendler, J. H., Dékány, I., Eds.; Kluwer: The Netherlands, 1996; pp 17−33.

(36) Lead references to studies of bimetallic nanoclusters in catalysis: (a) Au/Pt and Pd/Pt nanoclusters: Schmidt, G.; West, H.; Mehles, H.; Lenhert, A. *Inorg. Chem.* **1997**, *36*, 891 and refs 26 and 27 therein to layer migration phenomena. (b) Au/Pd and Pd/Au: Schmidt, G.; West, H.; Malm, J.-O.; Bovin, J.-O.; Grenthe, C. *Eur. Chem. J.* **1996**, *2*, 147. (c) Reetz, M. T.; Breinbrauer, R.; Wanninger, K. *Tet. Lett.* **1996**, *37*, 4499. (d) Pd/Ni: Toshima, N.; Lu, P. *Chem. Lett.* **1996**, 729. (e) Pt/Co: Yu, W.; Wang, Y.; Liu, H.; Zheng, W. *J. Mol. Catal. A: Chem.* **1996**, *112*, 105.

(37) Other lead references to the synthesis and characterization of bimetallic nanoclusters: (a) Pt/Pd oxide: Harada, M.; Asakura, K.; Ueki, Y.; Toshima, N. *J. Chem. Phys.* **1992**, *96*, 9730. Toshima, N.; Harada, M.; Yonezawa, T.; Kushihashi, K. Asakura, K. *J. Chem. Phys.* **1991**, *95*, 7448. Toshima, N.; Harada, M.; Yonezawa, T.; Hirai, H. *Chem. Lett.* **1989**, 1769. (b) Pt/Pd oxide: Kolbe, U.; Quaiser, S. A.; Winter, M.; Reetz, M. T. *Chem. Mater.* **1996**, *8*, 1889. (c) Pd/Ni, Fe/Co, Co/Ni: Reetz, M. T.; Helbig, W.; Quaiser, S. A. *Chem. Mater.* **1995**, *7*, 2227. (d) Au/Pt, Au/Pd: Schmid, G.; Lenhert, A.; Mulm, J.-O.; Bovin, J.-O. *Angew. Chem., Int. Engl. Ed.* **1991**, *30*, 874. (e) Pd/Cu: Bradley, J. S.; Hill, E. W.; Klein, C.; Chaduret, B.; Dutell, A. *Chem. Mater.* **1993**, *5*, 254. (f) Pt/Au: Sermon, P. A.; Thomas, J. M.; Keryou, K.; Millward, G. R. *Angew. Chem., Int. Eng. Ed.* **1987**, *26*, 918. (g) Pt/Ru: Richard, D.; Couves, J. W.; Thomas, J. M. *Faraday Discuss.* **1991**, *92*, 109.

recognized. For example, most bimetallic nanocluster syntheses simply mix together the two metals rather than adding them sequentially in a predetermined order designed to give a nanocluster with known layers (at least initially and in principle).[40] An experimental test of these suggestions is planned in the case of Ir/Rh and Pt/Pd polyoxoanion-stabilized nanoclusters, but we offer the *speculative* suggestions in Scheme 2 with the hope that they will stimulate others to test these ideas in their nanocluster systems as well.

Summary and Conclusions

In summary, the results herein provide the first mechanism-based insight into how to control the size of transition-metal nanoclusters formed under H_2 (and, by extension, with any other reducing agents that are eventually shown to operate by the autocatalytic surface-growth mechanism). Studies of other reductants are in progress.[41] Application of the mechanism-based principle of autocatalytic surface-growth and the living-metal−polymer phenomenon has permitted the rational synthesis of a series of transition-metal nanoclusters of prechosen average size. In addition, the use of the rate constant ratio $R' = k_2/k_1$ (M^{-1}) allowed us to survey our other nanocluster formation reactions and predict that the one with 7.5 equiv of excess polyoxoanion should give a nanocluster smaller than the $Ir(0)_{\sim 300}$ produced under our standard conditions. Then, just this reaction was used to prepare a distribution of nanoclusters centering about the previously missing, smaller member of the $Ir(0)_n$ magic-number series, $Ir(0)_{\sim 150}$. The R' method should be of use in explaining literature size-varied nanoclusters of different metals as well.[42] Also provided as part of this study is the first mechanism-based explanation for the preference for formation of so-called "magic-number" (closed-shell) size nanoclusters. The end result of the present work, a series of nanocluster distributions centering about four sequential magic numbers, $Ir(0)_{\sim 150}$, $Ir(0)_{\sim 300}$, $Ir(0)_{\sim 560}$, and $Ir(0)_{\sim 900}$, has not been previously reported. The principles involved should be extendible to any other transition metals and their combinations (vide supra) that are reducible by H_2 and that follow the autocatalytic surface-growth mechanism.

Last, one additional ramification of the autocatalytic surface-growth mechanism was discussed, namely, the many possibilities that exist for preparing a multitude of designed, initially onion-skinned structure, bi-, tri-, and higher multimetallic nanoclusters. Significantly, such a route is one where, at least in principle, *all possible geometric isomers* could be rationally prepared (Scheme 2), for a study of their catalytic, materials, and other physical properties. This additional, speculative prediction of the autocatalytic surface-growth mechanism and its associated living-polymer phenomenon remains to be tested, however.

Acknowledgment. The TEMs in this work were obtained with the expert assistance of Dr. Eric Schabtach at the University of Oregon's Microscopy Center. Helpful discussions and many references to micellar-template synthesized nanoclusters were provided by our colleague Professor Nancy Levinger; it is a pleasure to thank her. Financial support was provided by the Department of Energy, Chemical Sciences Division, Office of Basic Energy, grant DOE FG06-089ER13998.

Supporting Information Available: Figures A−F showing the TEMs which gave rise to the histograms shown in Figures 3−7, respectively (6 pages). See any current masthead page for ordering and Internet access instructions.

CM9704387

(38) (a) An initial "educated guess" about which of the possible onionskinned structures the thermodynamically preferred is offered here, but *only* as a "working hypotheses". Specifically, the expectation is that the transition metal (M) with the stronger M−M bond[38b,c] (i.e., the heavier metal) should tend to prefer the core of the nanocluster. Such a trend is already visible in the, for instance, Pt(core)/Pd (surface) bimetallic nanoclusters that have been recently made and structurally well characterized.[36a,b] (b) Conner, J. A. *Top. Curr. Chem.* **1997**, *71*, 71. See pp 76−78. (c) Pichler, G.; Skinner, H. A. In *The Chemistry of the Metal−Carbon Bond*; Hartley, F. R., Patai, S., Eds.; John Wiley: New York, 1982; see pp 76−80 and Table 13.

(39) A Cu_3Au alloy nanocluster: Sangregorio, C.; Galeotti, M.; Bardi, U.; Baglioni, P. *Langmuir* **1996**, *12* , 5800. Of interest to the present work is the statement therein that "we have no evidence on the mechanism that leads to mixing at the atomic level".

(40) In addition, the clear mechanistic prediction via Scheme 1 is that two different transition metals (with their different $E_{1/2}$ for reduction, and/or different rates of reduction) be reduced−that is, *nucleated*−at identical rates only by coincidence. In other words, an insight made possible by the present work is that literature bimetallic nanoclusters made under H_2, and where true alloys do not form, very likely contain the onionskin structures of Scheme 2.

(41) Widegren, J.; Watzky, M. A.; Finke, R. G., experiments in progress.

(42) (a) An interesting series of increasing size nanocolloids of different metals[4e] are those produced in the reference which follows:[42b] Os (<10 Å), Ir (14 Å), Pt(27 Å), Rh (40 Å), and Pd (53 Å). We'd expect that this series corresponds to an increasing R' ratio, although this remains to be verified or refuted. Note that it must be that these sizes are *kinetically controlled*, since the bulk metals are the thermodynamic product. Note also that the more electronegative, more easily reduced second row metals correspond to the larger sizes, as one would expect if they had larger k_2 values vs their third row counterparts. Note also that the reductant in these cases is typically an alcohol such as wet MeOH or 2-propanol, suggesting that alcohols are another class of reductants that are operating by the autocatalytic surface-growth mechanism. (b) Hirai, H.; Nakao, Y.; Toshima, N. *J. Macromol. Sci.-Chem.* **1979**, *A13*, 727.